Late Jurassic terrane collision in the northwestern margin of Gondwana (Cajamarca Complex, eastern flank of the Central Cordillera, Colombia)

Article *in* International Geology Review · November 2014

DOI: 10.1080/00206814.2014.963710

CITATIONS
75

READS
3,348

9 authors, including:

Idael F. Blanco-Quintero
University of Alicante
75 PUBLICATIONS **954** CITATIONS
SEE PROFILE

Antonio Garcia-Casco
University of Granada
229 PUBLICATIONS **4,309** CITATIONS
SEE PROFILE

L. M. Toro
University of Caldas
26 PUBLICATIONS **173** CITATIONS
SEE PROFILE

Mario Moreno-Sánchez
University of Caldas
54 PUBLICATIONS **359** CITATIONS
SEE PROFILE

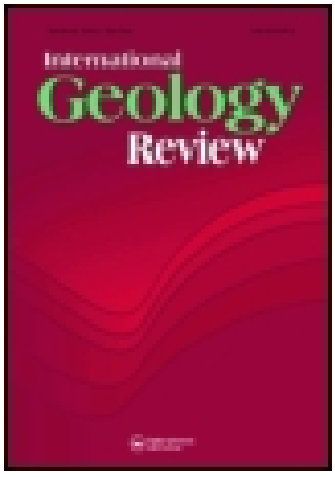

International Geology Review
Publication details, including instructions for authors and subscription information:
http://www.tandfonline.com/loi/tigr20

Late Jurassic terrane collision in the northwestern margin of Gondwana (Cajamarca Complex, eastern flank of the Central Cordillera, Colombia)

I. F. Blanco-Quintero[a], A. García-Casco[bc], L. M. Toro[d], M. Moreno[d], E. C. Ruiz[d], C. J. Vinasco[e], A. Cardona[f], C. Lázaro[b] & D. Morata[g]

[a] Programa de Geociencias, Universidad de los Andes, Bogotá, Colombia

[b] Departamento de Mineralogía y Petrología, Universidad de Granada, Granada, Spain

[c] Instituto Andaluz de Ciencias de la Tierra (IACT), CSIC-Universidad de Granada, Granada, Spain

[d] Departamento de Ciencias Geológicas, Universidad de Caldas, Manizales, Colombia

[e] Escuela de Geociencias y Medio Ambiente, Facultad de Minas, Universidad Nacional de Colombia, Medellín, Colombia

[f] Escuela de Procesos y Energía, Facultad de Minas, Universidad Nacional de Colombia, Medellín, Colombia

[g] Departamento de Geología y Centro de Excelencia en Geotermia de los Andes (CEGA, Fondap-Conicyt), Facultad de Ciencias Físicas y Matemáticas, Universidad de Chile, Santiago, Chile

Published online: 13 Oct 2014.

To cite this article: I. F. Blanco-Quintero, A. García-Casco, L. M. Toro, M. Moreno, E. C. Ruiz, C. J. Vinasco, A. Cardona, C. Lázaro & D. Morata (2014): Late Jurassic terrane collision in the northwestern margin of Gondwana (Cajamarca Complex, eastern flank of the Central Cordillera, Colombia), International Geology Review, DOI: 10.1080/00206814.2014.963710

To link to this article: http://dx.doi.org/10.1080/00206814.2014.963710

International Geology Review, 2014
http://dx.doi.org/10.1080/00206814.2014.963710

Late Jurassic terrane collision in the northwestern margin of Gondwana (Cajamarca Complex, eastern flank of the Central Cordillera, Colombia)

I. F. Blanco-Quintero[a]*, A. García-Casco[b,c], L. M. Toro[d], M. Moreno[d], E. C. Ruiz[d], C. J. Vinasco[e], A. Cardona[f], C. Lázaro[b] and D. Morata[g]

[a]*Programa de Geociencias, Universidad de los Andes, Bogotá, Colombia;* [b]*Departamento de Mineralogía y Petrología, Universidad de Granada, Granada, Spain;* [c]*Instituto Andaluz de Ciencias de la Tierra (IACT), CSIC-Universidad de Granada, Granada, Spain;* [d]*Departamento de Ciencias Geológicas, Universidad de Caldas, Manizales, Colombia;* [e]*Escuela de Geociencias y Medio Ambiente, Facultad de Minas, Universidad Nacional de Colombia, Medellín, Colombia;* [f]*Escuela de Procesos y Energía, Facultad de Minas, Universidad Nacional de Colombia, Medellín, Colombia;* [g]*Departamento de Geología y Centro de Excelencia en Geotermia de los Andes (CEGA, Fondap-Conicyt), Facultad de Ciencias Físicas y Matemáticas, Universidad de Chile, Santiago, Chile*

(*Received 3 September 2014; accepted 4 September 2014*)

Medium-grade metabasites and metapelites from the Cajamarca Complex (Central Cordillera of Colombia) are in fault contact with the Jurassic Ibague batholith and show a penetrative foliation, locally mylonitic, suggesting intense dynamic–thermal metamorphism. The amphibolites are composed of calcic amphibole + epidote + plagioclase + quartz plus rutile + titanite + apatite + carbonate as accessory phases. Chlorite and albite appear as retrograde replacements. The metapelites are mainly composed of phengite + quartz + garnet + chlorite, plus epidote + albite + apatite + titanite + haematite as accessory phases. Bulk geochemistry of the amphibolites indicates basaltic protoliths with a mid-ocean ridge basalt (MORB) signature, although enrichment in the mobile large-ion lithophile elements compared to MORB suggests pre- and/or syn-metamorphic alteration by fluids. Peak pressure–temperature determinations for both types of rocks are similar, ranging 550–580°C and 8 kbar (approximately 26 km depth and an apparent geothermal gradient of 22°C/km). ^{40}Ar-^{39}Ar dating of amphibole from two amphibolite samples and one phengitic mica from a pelitic schist yielded plateau ages of 146.5 ± 1.1 Ma and 157.8 ± 0.6 Ma, and 157.5 ± 0.4 Ma, respectively. These Late Jurassic ages contrast with previously published (Permian)Triassic ages of metamorphism in the Cajamarca Complex. Taken together, our data indicate tectonic-driven burial of oceanic supracrustal sequences down to mid-crustal depths during Late Jurassic times and are best explained as the result of terrane collision-related metamorphism and deformation in a fore-arc/volcanic-arc environment of the active western margin of Gondwana rather than as a result of Jurassic thermal–metamorphic resetting of a (Permian) Triassic metamorphic sequence during intrusion of the Jurassic Ibague batholith. Our results represent the first report of Jurassic terrane collision tectonics involving supracrustal oceanic rocks in the northwestern margin of Gondwana in Colombia.

Keywords: Cajamarca Complex; Central Cordillera; ^{40}Ar-^{39}Ar geochronology; dynamic–thermal metamorphism; collisional event

Introduction

Subduction of palaeo-Pacific-derived oceanic plates beneath the northwestern margin of Gondwana/South America (Colombia–Ecuador) has triggered significant accretion, extensive magmatism, and growth of the continental margin since late Palaeozoic amalgamation and subsequent mid-Jurassic fragmentation of Pangea (e.g. Restrepo and Toussaint 1982; Toussaint 1993; Vinasco *et al.* 2006; Cardona *et al.* 2010; Villagómez *et al.* 2011; Cochrane *et al.* 2014). Because of its long-lived convergence history, this margin constitutes an exceptional example for studying terrane accretion in a continental convergent setting. The Central Cordillera of Colombia records this tectonic evolution, where subduction, volcanic-arc magmatism, basin development and closure, and accretion of terrenes and redistribution of the accreted terranes through transcurrent systems have been recognized from the Permian to present (e.g. Restrepo and Toussaint 1982, 1988; Bayona *et al.* 2006, 2010; Vinasco *et al.* 2006; Kennan and Pindell 2009). In this evolution, two subduction/collision/accretion events triggering metamorphism are thought to have occurred during Permo–Triassic and mid to Late Cretaceous times (e.g. Vinasco *et al.* 2006; Bustamante *et al.* 2011), but evidence is lacking for Jurassic events in the Central Cordillera of Colombia.

In this work, we offer new major and trace element geochemistry, thermobarometric calculations, and ^{40}Ar-^{39}Ar dating of hornblende and muscovite from metabasite and metapelite samples collected in two areas of the Cajamarca Complex (Nelson 1962), between the towns of Ibague and Cajamarca and along the Combeima River. Our results are used to characterize the origin of the

*Corresponding author. Email: if.blanco@uniandes.edu.co

protoliths of the rocks, determine the metamorphic ages and conditions, and contribute to understanding the geodynamic evolution of this segment of the proto-Andean margin of Colombia where multiple tectonic events have shaped the continental margin since the Palaeozoic. We discuss the implications of a Jurassic age of orogenic metamorphism and evaluate the complex scenario of a convergent margin characterized by an essentially extensional volcanic-arc region (Aspden *et al*. 1987; Sarmiento-Rojas *et al*. 2006; Cochrane *et al*. 2014).

Geological setting

The geomorphology of the Colombian Andes is formed by three independent N–S-trending mountain ranges termed the Eastern, Central, and Western Cordilleras. The Eastern Cordillera consists of continental Precambrian and Palaeozoic metamorphic and igneous basement rocks covered by late Palaeozoic to Mesozoic sedimentary sequences (González *et al*. 1988) that record several stages of active and passive margin tectonics (Sarmiento-Rojas *et al*. 2006; Horton *et al*. 2010). The Central Cordillera, in contrast, mostly comprises continental-, oceanic-, and volcanic-arc-related Palaeozoic to Cretaceous magmatic rocks, generally metamorphosed to variable grade and intruded by Jurassic to Palaeogene volcanic-arc-related plutonic rock complexes (Restrepo and Toussaint 1982; Aspden *et al*. 1987; Maya and González 1995; Bayona *et al*. 2012). The Western Cordillera comprises allochthonous oceanic plateau and volcanic-arc sequences made of basic volcanic (and minor plutonic) rocks and marine sediments of Upper Cretaceous and Cenozoic age, intruded and covered by Cenozoic igneous rocks and volcanic sequences (Aspden *et al*. 1987; González *et al*. 1988; Kerr *et al*. 1997; Kerr and Tarney 2005; Villagómez *et al*. 2011).

The Central Cordillera (Figure 1A) is limited by the Otú-Pericos (to the east) and Cauca-Almaguer (to the west) strike-slip faults. On the western side, the San Jerónimo and Silvia–Pijao faults collectively define the Romeral fault system (Figure 1A), separating terranes of oceanic and continental affinity. The basement of the Central Cordillera is represented by low- to medium-grade metamorphic rocks of the Cajamarca Complex (Maya and González 1995) and high-grade rocks of the El Retiro Group and Las Palmas gneiss (González 2001). Other important lithostratigraphic/lithodemic complexes of the Central Cordillera are the mid-Cretaceous low/medium-grade metamorphic rocks of the oceanic Arquía complex and the unmetamorphosed volcano-sedimentary sequences of the volcanic-arc-related Early-to mid Cretaceous Quebradagrande complex (Figure 1A; Maya and González 1995; Nivia *et al*. 2006). All basement complexes are intruded and covered by Mesozoic–Tertiary plutonic and volcano-sedimentary rocks related to subduction of oceanic lithosphere from the west (Aspden *et al*. 1987).

Permian–Triassic metamorphic rocks of the Central Cordillera have different names, including the Cajamarca Group (Nelson 1962), Cajamarca Complex (Maya and González 1995), Tahami terrene (Toussaint and Restrepo 1989), Central Cordillera Polymetamorphic Complex (Toussaint and Restrepo 1989), and Cajamarca–Valdivia Terrane (Cediel *et al*. 2003). For simplicity, and because we have studied rocks located close to the classical location of Nelson (1962) and Maya and González (1995), in this work we use the term Cajamarca Complex. This complex includes pelitic schists, quartzites, marbles, and amphibolites (e.g. Maya and González 1995; González 2001). Antigorite-serpentinite blocks (approximately 2 km long) have been also described in the area (e.g. Gomez-Tapia and Bocanegra-Gomez 1999). The age of metamorphism was first described as Permian, but it was later defined as Mid to Late Triassic (ca. 240–230 Ma) based on the crystallization age of spatially associated syntectonic S-type granitoids and ^{40}Ar-^{39}Ar amphibole cooling ages of amphibolites in the northern segment of the Complex (Ordoñez-Carmona 2001; Vinasco *et al*. 2006; Restrepo *et al*. 2011; Cochrane *et al*. 2014). Older Devonian and younger Cretaceous ages have been also locally identified in rocks of the western flank of the Central Cordillera, but they have been grouped into other complexes (Table 6; Vesga and Barrero 1978; Núñez *et al*. 1979; González 1980; Sepulveda and Saldarriaga 1980; Restrepo *et al*. 1991; Restrepo *et al*. 2009; Villagómez *et al*. 2011).

Undeformed Meso–Cenozoic plutonic rocks and the modern volcanic arc intrude and cover the Cajamarca Complex. The elongated, weakly deformed I-type granitic Ibague Batholith (Nelson 1962) and banded gneisses and amphibolites of the Tierradentro complex (Figure 1A) limit the Cajamarca Complex to the east. The Tierradentro complex has poorly resolved and difficult-to-evaluate geochronological data (K-Ar hornblende ages ranging 171–226 Ma and K-Ar whole-rock age of 1360 ± 270; Barrero and Vesga 1976; Vesga and Barrero 1978; U-Pb SHRIMP and LA-ICP-MS zircon ages from quartz-gabbro and a granodiorite 236.3 ± 1.8 Ma and 243.13 + 5.4/–6.8 Ma, respectively; Bustamante *et al*. 2014). The Ibague Batholith and the corresponding volcanic sequence of Saldaña Formation (Bayona *et al*. 1994) are part of an extensive N–S elongated Jurassic magmatic belt that characterized the eastern segment of the Central Cordillera. This magmatic belt records at least three major magmatic peaks of ca. 195–180 Ma, 167–160 Ma, and 151–142 Ma (Aspden *et al*. 1987; Villagómez *et al*. 2011). U-Pb zircon crystallization ages for the Ibague Batholith are 166–169 Ma and 189 Ma (Villagómez *et al*. 2011). Published ^{40}Ar-^{39}Ar hornblende cooling ages of 182 Ma and 148 Ma overlap with this crystallization range,

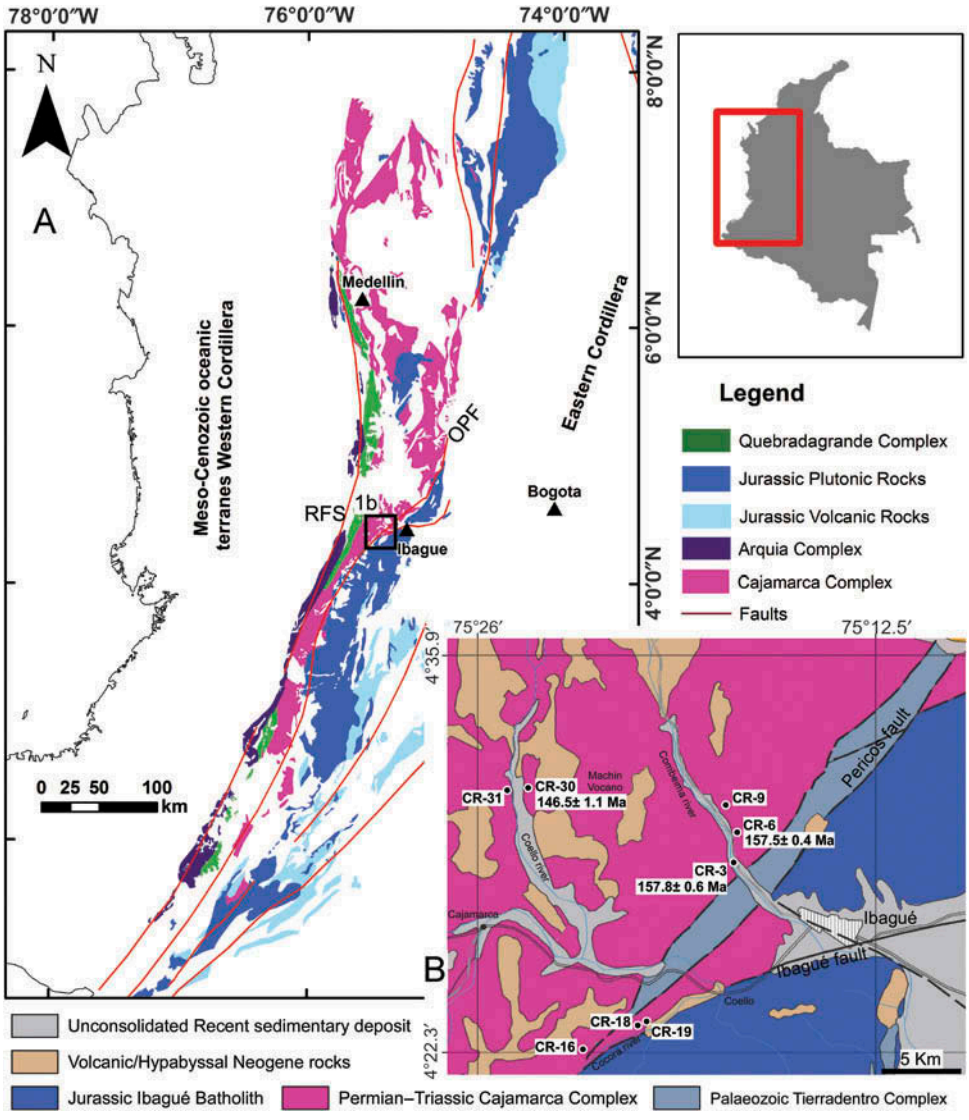

Figure 1. (A) Simplified geological map of Colombia showing the main units of the Central Cordillera. The inset shows the study area. RFS, Romeral fault system; OPF, Otú-Pericos Fault. (B) Geological map of the study area (modified after Núñez Tello 2001) showing the main geological units, with location of sample sites.

whereas Ar-Ar biotite cooling ages of 151 and 147 Ma and K/Ar hornblende and biotite ages of 150–140 Ma are younger (Vesga and Barrero 1978; Brook 1984; Aspden *et al*. 1987; Altenberger and Concha 2005). The upper limit of this volcanic activity is represented by an angular unconformity (Toussaint 1995), as indicated in the region by the polymictic conglomerate in the base of the sedimentary Yaví Formation (Toussaint 1995).

Two types of metamorphic rocks are exposed in the study area: abundant metabasites and intercalations of centrimetric to metric bands of pelitic schists (Figure 2A). These rocks show a strong penetrative foliation, locally related to mylonitization (i.e. grain-size reduction), which indicates intense dynamic–thermal metamorphism. Quartz ± carbonate veins crosscutting the regional foliation are common. All rocks are located to the west of the Otú-Pericos strike-slip fault and are nominally part of the Cajamarca Complex, as defined by Maya and González (1995). The studied rock package is in fault contact against the Ibague batholith and the Tierradentro complex (Figure 1B).

Analytical techniques

Bulk-rock chemistry

Fresh samples of amphibolite and metapelite lacking carbonate/quartz veins were selected for analyses. Powered whole-rock samples were obtained by grinding in a tungsten carbide mill. Major element and Zr compositions

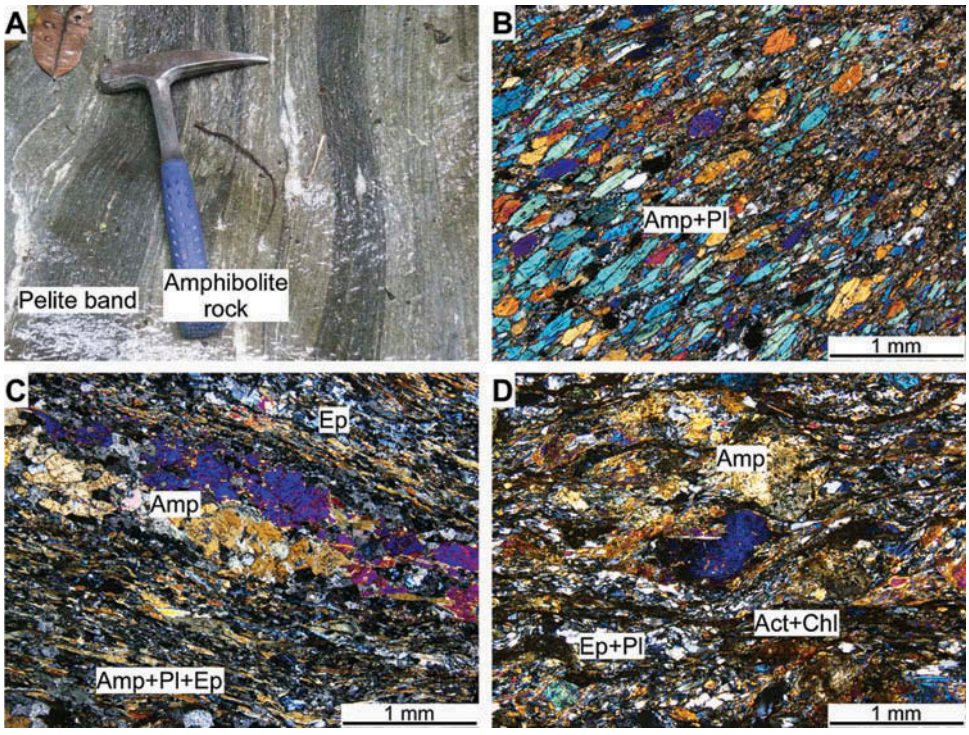

Figure 2. (A) Field view of amphibolites with layers of metapelite; the length of the hammer is 29 cm. Photomicrographs of amphibolite samples showing (B) strong penetrative foliation, (C) cataclastic amphibole, and (D) synkinematic amphibolite and late actinolite and chlorite replacing peak amphibole.

were determined on glass beads, made of 0.6 g of powered sample diluted in 6 g of $Li_2B_4O_7$, by Philips Magix Pro (PW-2440) X-ray fluorescence equipment at the University of Granada (Centro de Instrumentación Científica, CIC). Precision was better than ±1.5% for concentration of 10 wt.%. Precision for Zr and LOI was better than ±4% at 100 ppm concentration. The analyses were recalculated to an anhydrous 100 wt.% basis, and these data were used in the figures.

Trace elements, except Zr, were determined at the University of Granada (CIC) by ICP-Mass Spectrometry (ICP-MS) after HNO_3+HF digestion of 0.1000 g of sample powder in a Teflon-lined vessel at ~180°C and ~200 p.s.i. for 30 min, evaporation to dryness, and subsequent dissolution in 100 ml of 4 vol.% HNO_3. Blanks and international standards PMS, WSE, UBN, BEN, BR, and AGV (Govindaraju 1994) were run during analytical sessions. Precision was better than ±2% and ±5% for concentrations of 50 and 5 ppm.

Microprobe analyses

Major element composition of minerals was obtained by wavelength dispersive spectrometers with a CAMECA SX-100 microprobe (CIC, University of Granada), operated at 15 kV and 15 nA, with a beam size of 5 µm. The standards used for element calibrations were albite (Na), quartz (Si), periclase (Mg), sanidine (K), rutile (Ti), haematite (Fe), diopside (Ca), vanadinite (Cl), barite (Ba), fluorite (F), chromite (Cr), Al_2O_3 (Al), $MnTiO_3$ (Mn), and NiO (Ni). Amphibole composition was normalized following the scheme of Leake *et al*. (1997) and Fe^{3+} was estimated after the method of Schumacher (in Leake *et al*. 1997). Garnet composition was normalized to 8 cations and 12 oxygens, and Fe^{3+} was estimated by stoichiometry. Epidote and plagioclase were normalized to 12.5 and 8 oxygens, respectively, and assuming Fe(total) = Fe^{3+}. White mica and chlorite were normalized to 22 and 28 oxygens, respectively, and assuming Fe(total) = Fe^{2+}. The atomic concentration of elements per formula units is abbreviated apfu. The Mg number (Mg#) is expressed as the atomic ratio Mg/(Mg+Fe^{2+}). Mineral and end-member abbreviations are after Whitney and Evans (2010), with the end-members of phases written in the lower case.

Elemental X-ray images were obtained with the same CAMECA SX-100 microprobe of Granada University operated at 15 kV, 300 nA beam current, with step (pixel) size of 5 µm and counting time of 15 ms. The images were processed with Imager software (Torres-Roldán and García-Casco unpublished) and consist of the X-ray signals of Kα lines (except for Ba, Lα) of the elements (colour coded; expressed in counts/nA/s) corrected for 3.5 µs deadtime. The X-ray spectra of these

images were clipped to show the minerals of interest. The resulting images are overlain onto a grey-scale 'Z' image calculated by the sum of the products of the counts by atomic number (Si, Ti, Al, Fe, Mn, Mg, Ca, Na, Ba, K, Cr, Zn, and Cl) to show the basic textural relations of the scanned areas.

^{40}Ar-^{39}Ar determinations

Three hand-picked crystal separates (two hornblende amphibole and one muscovite separates, in the 250–100 μm size fraction) were analysed for Ar-Ar dating in the SERNAGEOMIN Laboratories, Chile. The separates were loaded in wells (3 × 3 mm, diameter × depth) in aluminium disks (18.5 × 4.8 mm, diameter × high). Fish Canyon Sanidine (FCS, 28.03 ± 0.1 Ma; Renne *et al.* 1994) was used as flux monitor. Samples were irradiated in the 5 MW Herald-type pool reactor in the Comisión Chilena de Energía Nuclear (Chile). After 2–3 weeks, samples were analysed by the total fusion and incremental heating methods. Once purified, the noble gasses were introduced into a high-resolution MAP 215–50 mass spectrometer equipped with an electron multiplier. Plateaus were defined according the approach of Fleck *et al.* (1977), which must comprise three or more sequential steps containing at least 50% of the total liberated ^{39}ArK, at the 2σ error level. Inverse isochrons are plotted using individual steps, and eliminating those considered suspect on the basis of visual inspection, mean square weighted deviate (MSWD) values <2, and unreasonable ^{36}Ar/^{40}Ar axis intercepts. For more details in the procedure and the correction factors, see Arancibia *et al.* (2006).

Mineral assemblages, textures, and mineral chemistry

Amphibolites

The amphibolites are fine- to medium-grained rocks, with millimetric bands of plagioclase and epidote within an amphibole matrix. The peak mineral association comprises hornblende + plagioclase + epidote + quartz. Hornblende amounts 50–60 modal per cent of the rock and appears strongly deformed along the main foliation (Figure 2B). The mineral association indicates epidote–amphibolite metamorphic facies. Not uncommonly, porphyroblastic amphibole appears deformed and crushed (Figure 2C and D), defining a tectonic lineation. The main phase of deformation and mylonitization occurred during and/or shortly after the metamorphic peak, as indicated by mineral composition (see next paragraphs). Plagioclase, epidote, and quartz occur in 15–20%, 10–15%, and 5% modal proportions, respectively, while titanite and, locally, carbonate are accessory phases. Partial retrogression is denoted by local formation of chlorite and actinolite both occurring as small matrix grains and at the rims of amphibole grains. Late carbonate-quartz-rich veins locally crosscut the foliation. Then, samples selected for mineral and whole-rock analysis are devoid of these veins and matrix carbonates.

The composition of peak amphibole is calcic and Fe rich (Figure 3A). In one sample (CR-3), peak amphibole reaches ferro-pargasite/ferro-edenite compositions (Figure 3A; Table 1) with $(Na+K)_A$ ranging 0.51–0.57 apfu and Mg# 0.41–0.45, while peak amphibole of other samples is ferro/magnesio-hornblende. These grains have low Si (6.36–6.53 apfu), moderate Al_{total} (2.13–2.34 apfu) and Ti (0.08–0.11 apfu; Figure 3B), and high Na_A (0.34–0.40 apfu) contents. Prograde cores and, mostly, retrograde crystals are of the actinolite-hornblende-tschermakite series ($(Na+K)_A$ < 0.5; Figure 3). The overall chemical variations are large (Al_{total} = 0.28–2.47 apfu, Si = 6.35–7.77 apfu, Ti = 0.01–0.14 apfu, and Mg# = 0.42–0.71), and the correlations of Ti-Si and Si-Mg# are negative and positive, respectively (Figure 3), in all aspects, suggesting a single prograde–retrograde *P–T* loop.

Epidote crystals form part of the peak assemblage (Figure 2C). They are not zoned and have moderate-to-high pistacite contents (Xps = Fe^{3+}/(Al-2)+Fe^{3+}] ranging from 0.48 to 0.69 (most abundant ~ 0.5) and low Mn (<0.1 apfu) contents (Table 2).

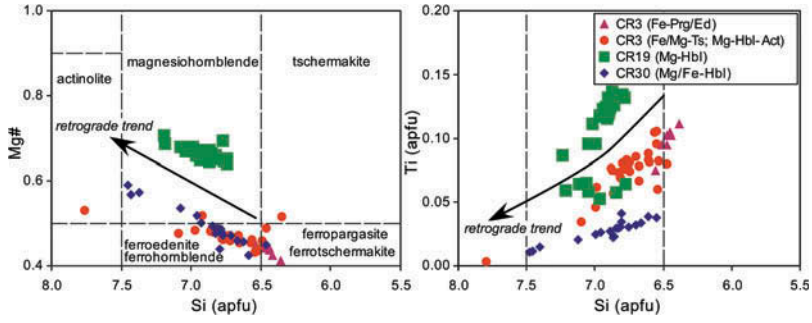

Figure 3. Composition of amphibole plotted in the classification scheme of Leake *et al.* (1997). The legend shows symbols as a function of amphibole composition. The abbreviations of end-members used are from Whitney and Evans (2010) and apfu means atomic concentration of elements per formula units.

Table 1. Representative analyses of amphibole (normalized to 22 O and 2 OH).

Sample	CR19	CR19	CR30	CR30	CR3	CR3	CR3	CR3	CR3	CR3
Type	MgHbl	MgHbl	FeHbl	MgHbl	MgHbl	Act	MgHbl	MgHbl	FePrg	FeEd
SiO_2	46.22	50.03	44.12	50.55	43.01	52.06	46.36	44.72	41.83	43.30
TiO_2	1.20	0.81	0.30	0.10	0.72	0.03	0.55	0.68	0.97	0.66
Al_2O_3	10.37	6.62	12.60	5.04	12.13	1.60	8.47	10.25	13.03	12.00
Cr_2O_3	0.12	0.13	0.02	0.01	0.05	0.02	0.05	0.01	0.06	0.08
FeO_{total}	13.84	12.84	19.03	16.31	19.29	19.30	19.59	19.15	20.01	19.15
MnO	0.32	0.24	0.29	0.31	0.26	0.24	0.25	0.23	0.26	0.25
MgO	12.27	14.39	7.91	12.07	8.15	11.34	9.66	8.82	7.26	8.14
NiO	0.02	0.01	0.00	0.01	0.00	0.02	0.00	0.03	0.00	0.01
CaO	11.49	11.66	10.73	11.79	11.76	12.34	11.22	11.83	11.77	11.94
BaO	0.02	0.02	0.00	0.02	0.01	0.00	0.01	0.01	0.03	0.00
Na_2O	1.12	0.75	1.58	0.59	1.29	0.08	0.71	1.17	1.50	1.30
K_2O	0.40	0.20	0.43	0.16	0.67	0.05	0.46	0.68	0.86	0.85
Total	97.51	97.83	97.13	97.11	97.51	97.25	97.54	97.77	97.80	97.89
Si	6.75	7.20	6.62	7.45	6.49	7.77	6.92	6.73	6.36	6.53
ivAl	1.25	0.80	1.38	0.55	1.51	0.23	1.08	1.27	1.64	1.47
total_T	8.00	8.00	8.00	8.00	8.00	8.00	8.00	8.00	8.00	8.00
vial	0.53	0.32	0.85	0.33	0.65	0.05	0.41	0.55	0.70	0.67
viTi	0.13	0.09	0.03	0.01	0.08	0.00	0.06	0.08	0.11	0.07
CrC	0.01	0.02	0.00	0.00	0.01	0.00	0.01	0.00	0.01	0.01
$Fe^{3+}C$	0.28	0.28	0.29	0.17	0.28	0.17	0.45	0.19	0.19	0.17
MgC	2.67	3.09	1.77	2.65	1.83	2.52	2.15	1.98	1.65	1.83
$Fe^{2+}C$	1.36	1.21	2.05	1.84	2.15	2.24	1.92	2.20	2.35	2.25
MnC	0.00	0.00	0.00	0.00	0.00	0.00	0.00	0.00	0.00	0.00
NiC	0.00	0.00	0.00	0.00	0.00	0.00	0.00	0.00	0.00	0.00
Total_C	5.00	5.00	5.00	5.00	5.00	4.98	5.00	5.00	5.00	5.00
MgB	0.00	0.00	0.00	0.00	0.00	0.00	0.00	0.00	0.00	0.00
$Fe^{2+}B$	0.04	0.05	0.05	0.01	0.01	0.00	0.07	0.01	0.01	0.00
MnB	0.04	0.03	0.04	0.04	0.03	0.00	0.03	0.03	0.03	0.03
CaB	1.80	1.80	1.73	1.86	1.90	1.97	1.79	1.91	1.92	1.93
NaB	0.12	0.12	0.19	0.09	0.05	0.02	0.10	0.05	0.04	0.04
Total_B	2.00	2.00	2.00	2.00	2.00	2.00	2.00	2.00	2.00	2.00
NaA	0.19	0.09	0.27	0.08	0.33	0.00	0.10	0.29	0.40	0.34
BaA	0.00	0.00	0.00	0.00	0.00	0.00	0.00	0.00	0.00	0.00
KA	0.07	0.04	0.08	0.03	0.13	0.01	0.09	0.13	0.17	0.16
Total_A	0.27	0.13	0.35	0.11	0.45	0.01	0.19	0.42	0.57	0.51
Mg#	0.66	0.71	0.46	0.59	0.46	0.53	0.52	0.47	0.41	0.45

Note: Amphibole type is referred as Mg/Fe hornblende (MgHbl, FeHbl), Fe-pargasite (FePrg), Fe-edenite (FeEd), and actinolite (Act).

Table 2. Representative analyses of epidote, chlorite, and garnet (normalized to 12 O and 1 OH, 20 O and 16 OH, and 12 O, respectively).

Sample	CR30	CR30	CR30	CR-6	CR19	CR30	CR-6	CR-6	CR-6	CR-6	CR-6	CR-6
Type	Amph	Amph	Amph	Mpel	Amph	Amph	Mpel	Mpel	Mpel	Mpel	Mpel	Mpel
Mineral	Ep	Ep	Ep	Ep	Chl	Chl	Chl	Chl	Chl	Grt	Grt	Grt
SiO_2	38.31	38.55	37.49	37.77	28.18	25.72	27.42	27.80	25.57	36.98	37.31	37.26
TiO_2	0.21	0.19	0.16	0.11	0.10	0.05	0.07	0.10	0.07	0.13	0.13	0.07
Al_2O_3	26.89	27.30	26.49	27.64	19.60	21.05	22.56	23.48	21.46	20.72	20.96	21.00
Cr_2O_3	0.01	0.00	0.06	0.00	0.01	0.00	0.04	0.03	0.00	0.02	0.00	0.00
FeO_{total}	7.60	7.14	7.35	6.34	19.19	27.44	23.49	23.12	25.63	16.57	22.54	23.87
MnO	0.10	0.10	0.19	0.36	0.31	0.36	0.79	0.86	0.64	19.59	10.53	11.05
MgO	0.02	0.03	0.04	0.07	19.34	12.51	12.71	12.09	14.56	0.56	0.81	0.88
NiO	0.02	0.02	0.00	0.04	0.01	0.01	0.01	0.04	0.02	0.00	0.00	0.01
CaO	23.55	23.43	23.50	22.24	0.11	0.06	0.02	0.00	0.00	5.69	8.45	7.04

(*Continued*)

Table 2. (Continued).

Sample	CR30	CR30	CR30	CR-6	CR19	CR30	CR-6	CR-6	CR-6	CR-6	CR-6	CR-6
Type	Amph	Amph	Amph	Mpel	Amph	Amph	Mpel	Mpel	Mpel	Mpel	Mpel	Mpel
Mineral	Ep	Ep	Ep	Ep	Chl	Chl	Chl	Chl	Chl	Grt	Grt	Grt
BaO	0.00	0.01	0.02	0.00	0.02	0.00	0.08	0.02	0.00	0.03	0.00	0.00
Na_2O	0.00	0.01	0.00	0.01	0.07	0.00	0.02	0.04	0.00	0.05	0.02	0.01
K_2O	0.02	0.01	0.01	0.03	0.02	0.04	0.99	1.22	0.01	0.00	0.01	0.02
Total	96.83	96.89	95.32	94.61	87.09	87.38	88.38	88.94	88.11	100.44	100.93	101.37
Si	3.00	3.01	2.99	3.01	5.78	5.51	5.69	5.71	5.39	2.99	2.98	2.97
Ti	0.01	0.01	0.01	0.01	0.02	0.01	0.01	0.02	0.01	0.01	0.01	0.00
Al	2.49	2.52	2.49	2.60	4.74	5.31	5.52	5.69	5.33	1.97	1.97	1.97
Cr	0.00	0.00	0.00	0.00	0.00	0.00	0.01	0.00	0.00	0.00	0.00	0.00
Fe^{3+}	0.50	0.47	0.49	0.42	0.00	0.00	0.00	0.00	0.00	0.04	0.06	0.08
Fe^{2+}	0.00	0.00	0.00	0.00	3.29	4.92	4.08	3.97	4.52	1.08	1.45	1.52
Mn	0.01	0.01	0.01	0.02	0.05	0.06	0.14	0.15	0.11	1.34	0.71	0.75
Mg	0.00	0.00	0.01	0.01	5.91	3.99	3.93	3.70	4.57	0.07	0.10	0.10
Ni	0.00	0.00	0.00	0.00	0.00	0.00	0.00	0.01	0.00	0.00	0.00	0.00
Ca	1.98	1.96	2.01	1.90	0.03	0.01	0.00	0.00	0.00	0.49	0.72	0.60
Ba	0.00	0.00	0.00	0.00	0.00	0.00	0.01	0.00	0.00	0.00	0.00	0.00
Na	0.00	0.00	0.00	0.00	0.03	0.00	0.01	0.01	0.00	0.01	0.00	0.00
K	0.00	0.00	0.00	0.00	0.01	0.01	0.26	0.32	0.00	0.00	0.00	0.00
Mg#					0.64	0.45	0.49	0.48	0.50	0.06	0.06	0.06
Xpist	0.51	0.48	0.50	0.41								
Xalm										0.36	0.49	0.51
XSps										0.45	0.24	0.25
XPrp										0.02	0.03	0.04
XGrs										0.17	0.24	0.20
XGrs (excluding Mn)										0.30	0.32	0.27

Note: Sample type is referred as amphibolite (Amph) and metapelite (Mpel).

The most common composition of plagioclase is albite (Xan = 0.02–0.05) with low potassium contents (Xor < 0.02; Table 3). Sample CR19 has plagioclase with andesine–labradorite compositions (Xan = 0.36–0.56, XOr < 0.01; Table 3).

Chlorite has Mg# = 0.45–0.64, Si = 5.45–6.35, and Al = 4.36–5.32 apfu. The Mn content is low, up to 0.07 apfu (Table 3). The chemical variations of chlorite are mainly due to the combination of the Tschermak (Mg, Fe) $Si^{VI}Al_{-1}{}^{IV}Al_{-1}$ and $FeMg_{-1}$ exchange vectors. Chlorite is

Table 3. Representative analyses of plagioclase and phengitic muscovite (normalized to 8 O and 22 O and 4 OH, respectively).

Sample	CR3	CR3	CR19	CR30	CR30	CR-6	CR-6	CR-6	CR-6
Type	Amph	Amph	Amph	Amph	Amph	Mpel	Mpel	Mpel	Mpel
Mineral	Pl	Pl	Pl	Pl	Pl	Pl	Pl	Ms	Ms
SiO_2	67.92	68.65	55.74	67.30	66.50	65.83	69.17	49.76	47.33
TiO_2	0.00	0.00	0.00	0.02	0.02	0.00	0.00	0.22	0.36
Al_2O_3	19.77	20.28	28.02	19.46	19.66	21.21	19.61	29.90	32.75
Cr_2O_3	0.00	0.00	0.00	0.02	0.00	0.02	0.01	0.03	0.09
FeO	0.14	0.11	0.20	0.21	0.07	0.22	0.13	2.88	2.15
MnO	0.00	0.00	0.04	0.00	0.00	0.01	0.00	0.06	0.04
MgO	0.00	0.01	0.01	0.00	0.00	0.00	0.00	2.79	1.71
NiO	0.03	0.00	0.00	0.05	0.02	0.04	0.00	0.00	0.00
CaO	0.41	0.43	10.17	0.65	1.04	1.98	0.11	0.00	0.00
BaO	0.01	0.00	0.00	0.00	0.00	0.00	0.00	0.16	0.42
Na_2O	11.50	11.32	5.80	11.84	11.57	10.37	11.52	0.50	0.34
K_2O	0.07	0.30	0.05	0.06	0.08	0.11	0.09	9.17	9.91
Total	99.86	101.14	100.13	99.62	98.96	99.83	100.66	95.64	95.23

(*Continued*)

Table 3. (Continued).

Sample	CR3	CR3	CR19	CR30	CR30	CR-6	CR-6	CR-6	CR-6
Type	Amph	Amph	Amph	Amph	Amph	Mpel	Mpel	Mpel	Mpel
Mineral	Pl	Pl	Pl	Pl	Pl	Pl	Pl	Ms	Ms
Si	2.98	2.97	2.51	2.97	2.95	2.90	3.00	6.60	6.33
Ti	0.00	0.00	0.00	0.00	0.00	0.00	0.00	0.02	0.04
Al	1.02	1.03	1.49	1.01	1.03	1.10	1.00	4.68	5.16
Cr	0.00	0.00	0.00	0.00	0.00	0.00	0.00	0.00	0.01
Fe^{3+}	0.01	0.00	0.01	0.01	0.00	0.01	0.00		
Fe^{2+}			0.00					0.32	0.24
Mn	0.00	0.00	0.00	0.00	0.00	0.00	0.00	0.01	0.00
Mg	0.00	0.00	0.00	0.00	0.00	0.00	0.00	0.55	0.34
Ni	0.00	0.00	0.00	0.00	0.00	0.00	0.00	0.00	0.00
Ca	0.02	0.02	0.49	0.03	0.05	0.09	0.01	0.00	0.00
Ba	0.00	0.00	0.00	0.00	0.00	0.00	0.00	0.01	0.02
Na	0.98	0.95	0.51	1.01	1.00	0.89	0.97	0.13	0.09
K	0.00	0.02	0.00	0.00	0.00	0.01	0.01	1.55	1.69
Ab	0.98	0.96	0.51	0.97	0.95	0.90	0.99		
An	0.02	0.02	0.49	0.03	0.05	0.09	0.01		
Or	0.00	0.02	0.00	0.00	0.00	0.01	0.01		
Mg#								0.63	0.59

Note: Sample type is referred as amphibolite (Amph) and metapelite (Mpel).

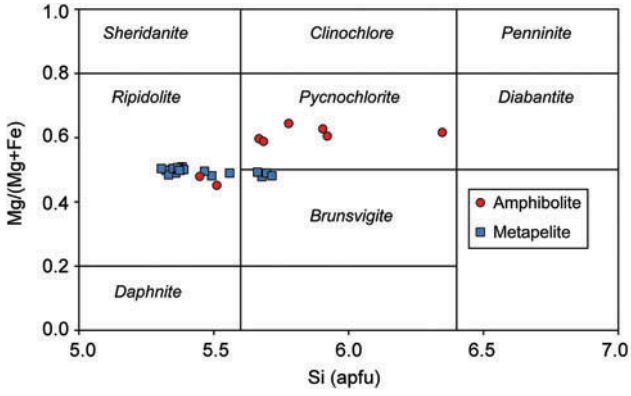

Figure 4. Chlorite composition in the classification diagram of Hey (1954).

ripidolite-pycnochlorite according to the Si and Mg# contents (Figure 4; Hey 1954).

Metapelites

The metapelites are fine- to medium-size grained schists (Figure 5A). They are mainly composed of phengite (20–30%) + quartz (50–60%) + garnet (0–10%) + chlorite (10–12%) (Figure 5B), plus epidote + albite + apatite + titanite + haematite as accessory phases. Phengitic mica defines the main S1 foliation and a second crenulation S2 foliation (Figure 5C and D). Significant chemical variations in phengite as function of structural/textural position are not detected (Figure 5D). Quartz and chlorite also define the main foliation. The garnet porphyroblasts, up to 1 mm in diameter, show irregular edges (Figure 5E and F), while Fe-oxides appear in veins following the foliation.

Potassic white mica is phengite (Rieder *et al*. 1998), with high Si (6.16–6.60 apfu), Mg (0.27–0.55 apfu), Fe (0.21–0.42 apfu), and moderate Al (4.68–5.46 apfu) contents (Figure 6; Table 3). The crystals have low Na (up to 0.13 apfu) and Ba (< 0.02 apfu) contents. The principal deviations of composition from the pure muscovite end-member are due to the Tschermak substitution (Mg,Fe) $Si^{VI}Al_{-1}{}^{IV}Al_{-1}$, implying an important increase in Mg, Fe, and Si (Figure 6, Table 3). The compositions with the highest phengite content suggest relatively high pressure during the crystal growth.

Garnet porphyroblasts are rich in almandine (Xalm = 0.35–0.51) and spessartine (Xsps = 0.24–0.45; Figure 7A) and to some extent grossular (Xgrs = 0.17–0.24; Table 2) and are poor in pyrope (Xprp <0.04). The highest Xsps contents are recorded in the cores, decreasing towards the rims where the highest Mg# (0.06) is recorded (Figure 7B). This pattern is characteristic of prograde growth zoning.

Chlorite has Si = 5.30–5.71 apfu and Al = 5.05–5.69 apfu and Mg# = 0.4–0.51, with low Mn (0.11–0.22 apfu) content. Chlorite is ripidolite-brunsvigite according to the Si and Mg# = 0.4–0.51 contents (Hey 1954).

Finally, epidote grains are minor and small and have Fe^{3+} = 0.42 apfu (Table 2). Small crystals of plagioclase are mostly pure albite (Xan = 0.10–0.01; Table 3) occurring parallel to the main foliation. Titanite has low Al contents (0.06–0.09 apfu).

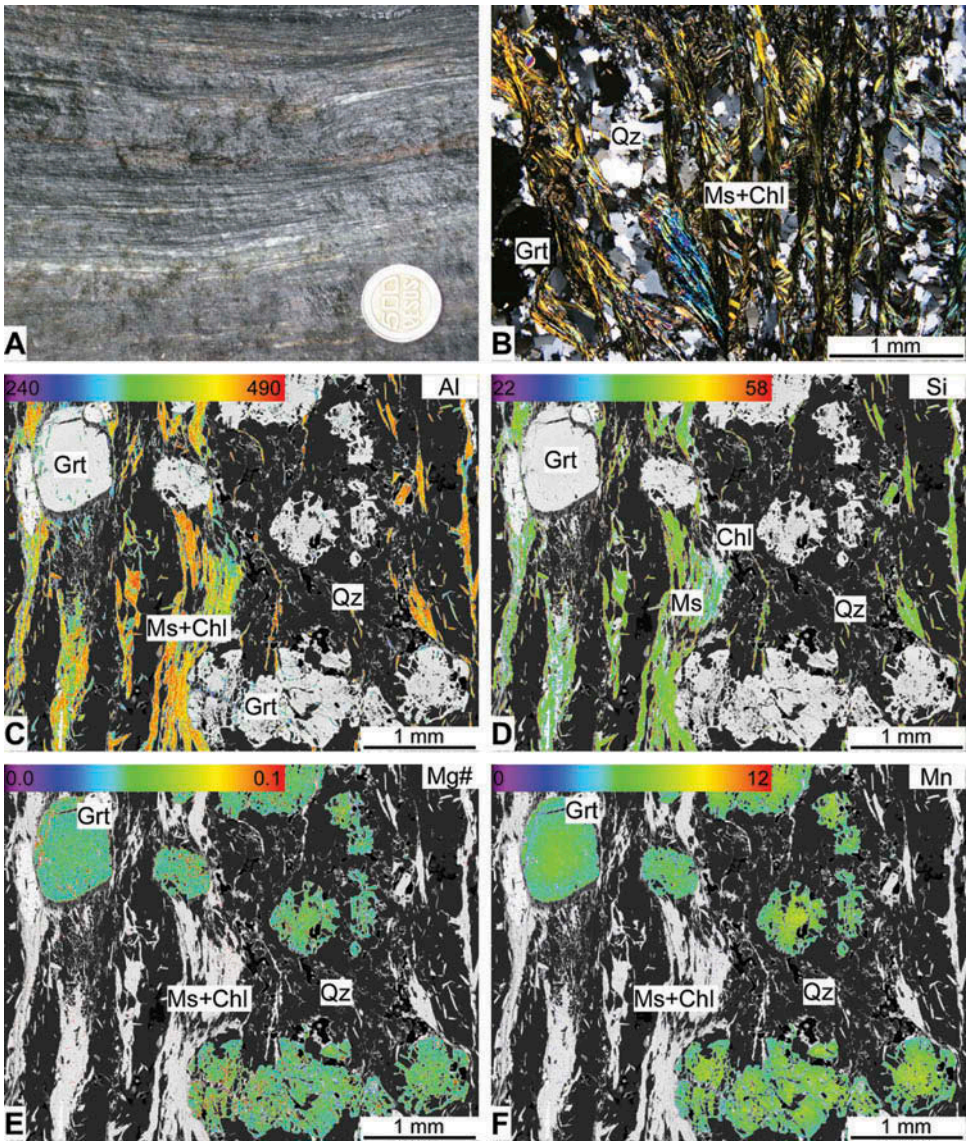

Figure 5. (A) Outcrop of foliated pelitic schist (coin diameter is 23 mm); (B) photomicrograph of a typical metapelite composed of quartz, muscovite, chlorite, and garnet; (C) Al-Kα X-ray image showing the intergrowths of synkinematic muscovite (orange) and chlorite (blue); (D) Si-Kα X-ray image of muscovite and chlorite; (E) Mg# (Mg/(Mg+Fe)-Kα) X-ray image for garnet showing smooth zoning; (F) Mn-Kα X-ray image of concentric zoned garnet showing Mn-richer cores and prograde Mn-poor rims. In all XR images, the colour scale bar is in counts/nA/s.

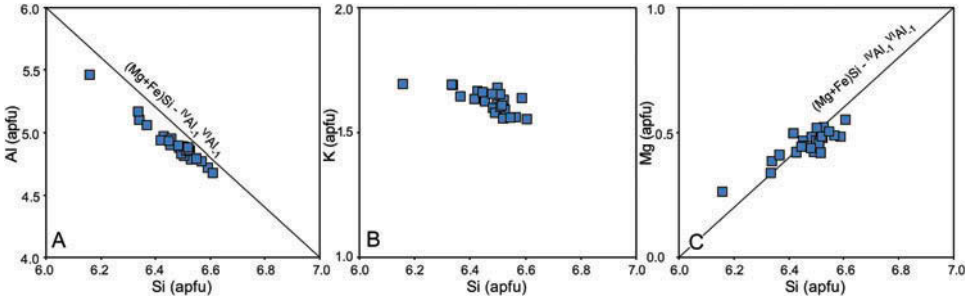

Figure 6. Chemical variation of phengitic muscovite. Si *versus* (A) Al, (B) K, (C) Mg (atoms per 22 oxygens); the Tschermak substitution vector is shown for reference.

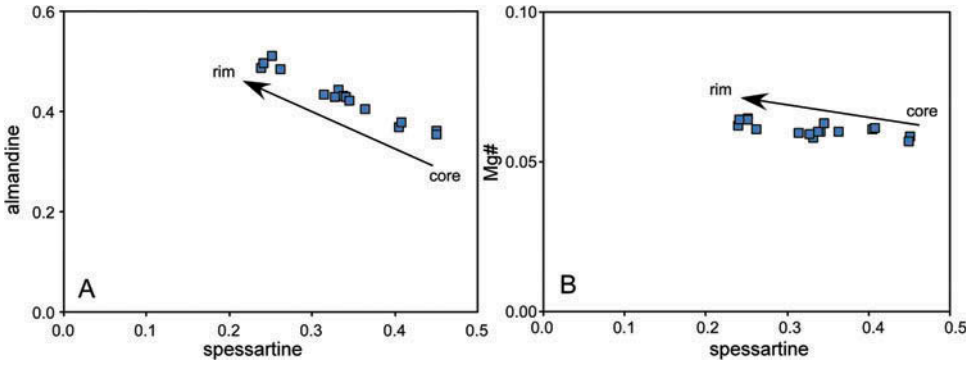

Figure 7. Spessartine content (mole fraction) *versus* (A) almandine and (B) Mg# content of garnet.

P–T Conditions

Isochemical *P–T* projections (pseudosections) were calculated for representative bulk-rock compositions of the two groups of rocks studied. The results were compared with the observed mineral assemblages. The pseudosection for metapelite CR-6 (Table 4) was calculated in the KNCFMASH system using Perple_X software (Connolly 2005). A fluid phase, assumed to be pure H_2O, was considered in excess. The solution models used for plagioclase, chlorite, white mica, and garnet are those of Newton *et al*. (1980); Holland *et al*. (1998), Coggon and Holland (2002), and Holland and Powell (1998),

Table 4. Major (wt.%) and trace (ppm) element composition of the study samples.

Sample	CR9	CR16	CR19	CR30	CR31	CR6
Type	Amph	Amph	Amph	Amph	Amp	Mpel
SiO_2	48.57	44.69	45.05	48.93	46.69	66.96
TiO_2	1.54	2.52	1.36	2.17	1.59	1.02
Al_2O_3	14.35	15.07	15.43	14.39	16.45	12.61
Fe_2O_{3tot}	11.86	13.09	10.98	13.99	11.06	7.77
MnO	0.20	0.17	0.21	0.20	0.18	0.34
MgO	8.16	7.28	8.75	5.62	6.41	3.24
CaO	9.21	10.59	8.82	9.46	12.70	0.84
Na_2O	2.61	1.99	1.68	1.98	1.60	0.09
K_2O	0.10	1.04	0.34	0.16	0.08	2.56
P_2O_5	0.13	0.31	0.11	0.18	0.19	0.07
LOI	2.65	2.52	7.32	2.13	2.15	3.98
total	99.39	99.27	100.05	99.21	99.10	99.48
Li	18.85	15.69	34.76	13.85	7.92	
Rb	1.61	19.80	5.25	3.58	0.94	
Cs	0.35	0.70	0.79	0.15	0.09	
Be	2.36	1.51	3.86	0.92	0.61	
Sr	72.92	316.87	66.81	116.87	206.01	
Ba	10.89	200.26	34.02	38.49	15.45	
Sc	49.43	38.72	42.58	47.47	40.34	
V	314.01	313.58	230.05	424.79	286.50	
Cr	284.86	109.00	310.19	41.97	293.29	
Co	84.45	53.36	40.24	43.41	47.90	
Ni	79.29	56.59	91.35	28.40	81.50	
Cu	64.12	19.59	44.38	52.35	47.17	
Zn	117.03	118.60	118.26	120.68	90.79	
Ga	13.85	21.61	13.75	20.80	17.89	
Y	35.51	29.29	23.40	43.60	32.87	
Nb	2.85	17.44	0.61	5.53	4.23	
Ta	0.75	1.37	0.38	0.57	0.49	
Zr	86.50	176.50	66.90	130.50	114.50	
Hf	1.13	0.62	1.42	0.80	0.78	

(*Continued*)

Table 4. (Continued).

Sample	CR9	CR16	CR19	CR30	CR31	CR6
Type	Amph	Amph	Amph	Amph	Amp	Mpel
Mo	10.67	1.73	3.17	2.07	3.66	
Sn	1.57	2.01	2.27	1.37	1.18	
Tl	0.36	0.18	0.56	0.10	0.04	
Pb	1.19	1.63	14.42	0.98	0.63	
U	0.38	0.37	0.61	0.19	0.14	
Th	0.46	1.37	0.71	0.51	0.35	
La	3.51	15.16	1.79	6.60	5.38	
Ce	10.30	35.00	4.47	17.52	15.34	
Pr	1.92	4.82	1.07	2.85	2.47	
Nd	11.54	21.72	8.08	14.34	12.59	
Sm	4.59	5.80	4.17	4.96	3.74	
Eu	1.60	2.02	1.28	1.78	1.37	
Gd	5.59	6.25	4.98	6.44	5.06	
Tb	1.12	1.01	0.89	1.19	0.91	
Dy	6.61	5.49	4.98	7.43	5.45	
Ho	1.35	1.08	0.97	1.58	1.19	
Er	4.22	2.88	3.52	4.54	3.32	
Tm	0.71	0.43	0.62	0.70	0.50	
Yb	3.91	2.53	3.44	4.26	3.01	
Lu	0.60	0.33	0.63	0.58	0.40	

Note: Sample type is referred as amphibolite (Amph) and metapelite (Mpel).

respectively. The pseudosection (Figure 8A) shows a field with the association Qz + Ms + Grt + Chl + Ep, consistent with observed mineral assemblages in metapelites. To further constrain the *P–T* conditions, mineral composition isopleths for garnet (Mg# and grossular) were determined (Figure 8A), confirming the field. Because MnO was not included in the calculations, the end-member proportions were recalculated (Table 2), showing grossular contents around 0.28–0.32 and Mg# around 0.06, which result in a *P–T* determination by intercept of the isopleths at approximately 550ºC and 8.2 kbar. During retrogression, albite is formed, as indicated by the phase associations (Figure 8A).

The pseudosection for metabasite sample CR-19 (Table 4) was calculated in the NCFMASHT system using the Perple_X software (Connolly 2005). A fluid phase, assumed to be pure H_2O, was considered in excess. The solution models used are those used for the metapelite sample plus the amphibole model of Dale *et al*. (2005) and an ideal model for ilmenite-haematite. The result is shown in Figure 8B, including mineral composition isopleths for amphibole (Mg#) and plagioclase (Xan). The field of the assemblage amphibole + zoisite + plagioclase + quartz plus minor rutile and chlorite is large. Using amphibole and plagioclase composition isopleths, the conditions calculated correspond to approximately 8 kbar and 580ºC, similar to those calculated for metapelite sample CR-6. In both cases, a clockwise prograde heating+burial path followed by cooling and exhumation is inferred.

Whole-rock composition

The amphibolites are basaltic in composition, of the subalkaline series in the TAS diagram (Figure 9A; Le Maitre *et al*. 1989), with SiO_2 ranging between 46.83 and 51.14 wt.% and alkali elements (Na_2O+K_2O) between 1.75 and 3.17 wt.%. However, due to possible fluid–rock interactions before and during metamorphism, changes in the magmatic bulk-rock composition cannot be ruled out. For this reason, the diagrams used here are based on elements that are least likely to be mobile during metamorphism. In the Zr/TiO_2 *versus* Nb/Y classification diagram (Winchester and Floyd 1977), the amphibolites plot as basalt/subalkaline basalt (Figure 9B).

Harker diagrams for amphibolites are presented in Figure 10. In general, the amphibolites have high Al_2O_3 and TiO_2 contents (Table 4 and Figure 10), showing negative correlation trends with SiO_2. The rocks are also rich in FeO_{tot} and MgO and are poor in Na_2O and K_2O (Table 4), indicating low- to medium-K affinity (Peccerillo and Taylor 1976). The Mg# is relatively low (0.30–0.47). Compared to the metabasites, the metapelite shows high SiO_2 (70.69 wt.%) and K_2O (2.70 wt.%) contents and very low Na_2O (0.10 wt.%) and CaO (0.89 wt.%; Figure 10; Table 4) contents.

Normalized to chondrite (McDonough and Sun 1995), rare earth element (REE) patterns in the metabasites are flat or slightly depleted in LREEs (Figure 11A), except for sample CR-16 which is enriched in the LREEs. The (La/Yb)*n* ratio varies from 0.35 to 1.22, while sample CR-16

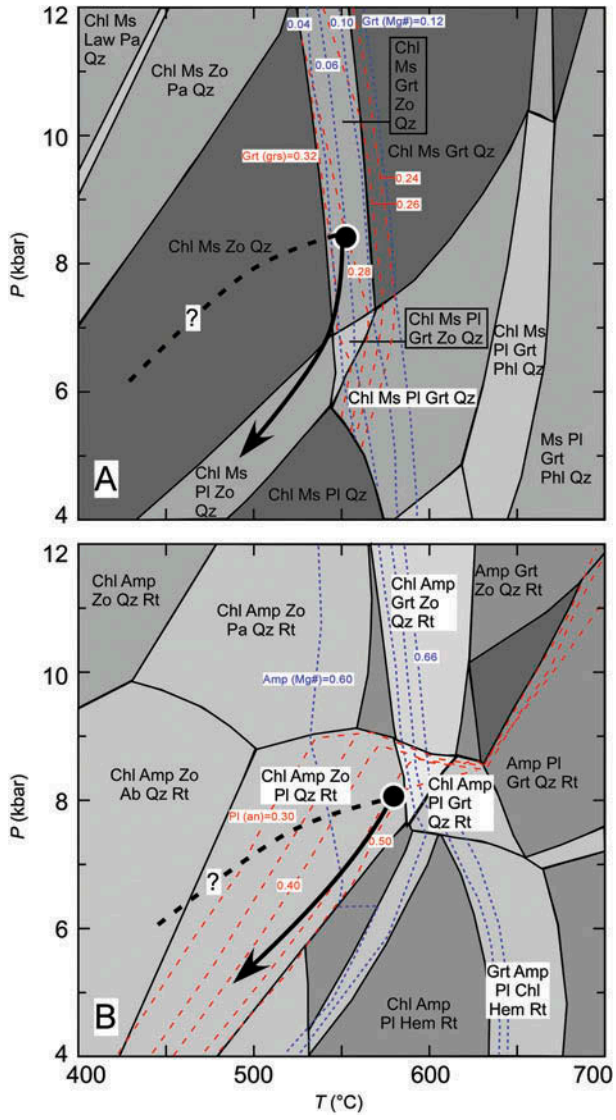

Figure 8. *P–T* conditions of studied rocks. (A) Pseudosection for metapelite sample CR-6; the isopleths for garnet are indicated for Mg# as dotted lines and grossular as dashed lines. (B) Pseudosection for amphibolite sample CR-19; the composition isopleths are indicated for Mg# in amphibole as dotted lines and anorthite contents in plagioclase as dashed lines.

yields values as high as 4.07, suggesting more fractionated REEs. Most samples yield a slight negative Eu anomaly (Eu/Eu* = 0.86–0.96), while sample CR-16 shows a slightly positive value around 1.02.

In the N-MORB-normalized element diagram (N-MORB after Sun and McDonough 1989), the amphibolites show negative slopes, with slightly flat patterns for the high-field strength elements (HFSEs) (Figure 11B). The samples show enrichment in the large-ion lithophile elements (LILEs) compared to N-MORB patterns (Figure 11B), mainly in Cs, Rb, Ba, and Pb. A positive anomaly in Pb is seen, particularly in sample CR-19 (Figure 11B), which also is depleted in Nb, La, and Ce.

^{40}Ar-^{39}Ar ages

^{40}Ar-^{39}Ar age determinations are presented in Table 5 and Figure 12. All analysed mineral separates, including a phengitic mica (from metapelite sample CR-6) and the two hornblendes (from amphibolite samples CR-3 and CR-30), yielded well defined plateau ages.

The plateau age of phengitic mica is 157.5 ± 0.4 Ma (98.1% Ar released, MSWD 0.65). Integrated and isochron ages are similar (157.3 ± 0.4 and 157.6 ± 0.6 Ma, respectively) with a $^{40}Ar/^{36}Ar$ intercept of 287 ± 13 Ma. Amphibole from sample CR-3 yields a plateau age of 157.8 ± 0.6 Ma (97.4% Ar released, MSWD 0.44). Results of integrated and isochron ages are only slightly different, 161.2 ± 0.7 and 159 ± 4 Ma, respectively, with intercept of 260 ± 60 Ma. Amphibole from sample CR-30 yields a plateau age of 146.5 ± 1.1 Ma (96% Ar released, MSWD 0.75). Integrated and isochron ages are similar (147.2 ± 1.3 and 146.5 ± 1.4 Ma, respectively) with a $^{40}Ar/^{36}Ar$ intercept of 296 ± 3 Ma.

The similarity of these ages and the lack of excess Ar allow using the plateau ages in all cases. Summarizing, the data indicate 157.5 ± 0.4 Ma and 157.8 ± 0.6 Ma and 146.5 ± 1.1 Ma for muscovite in sample CR-6 and amphibole of samples CR-3 and CR-30, respectively.

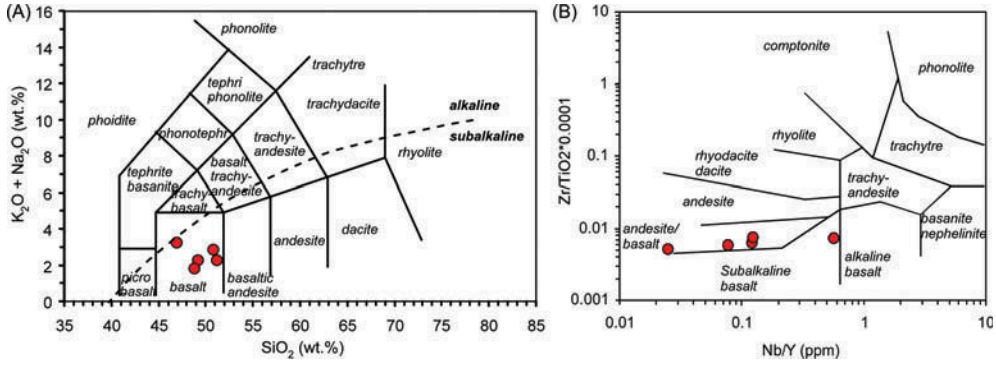

Figure 9. Composition of studied amphibolite samples in the (A) TAS classification of volcanic rocks (Le Maitre *et al*. 1989) and (B) Zr/Ti *versus* Nb/Y classification diagram based on immobile element (Winchester and Floyd 1977).

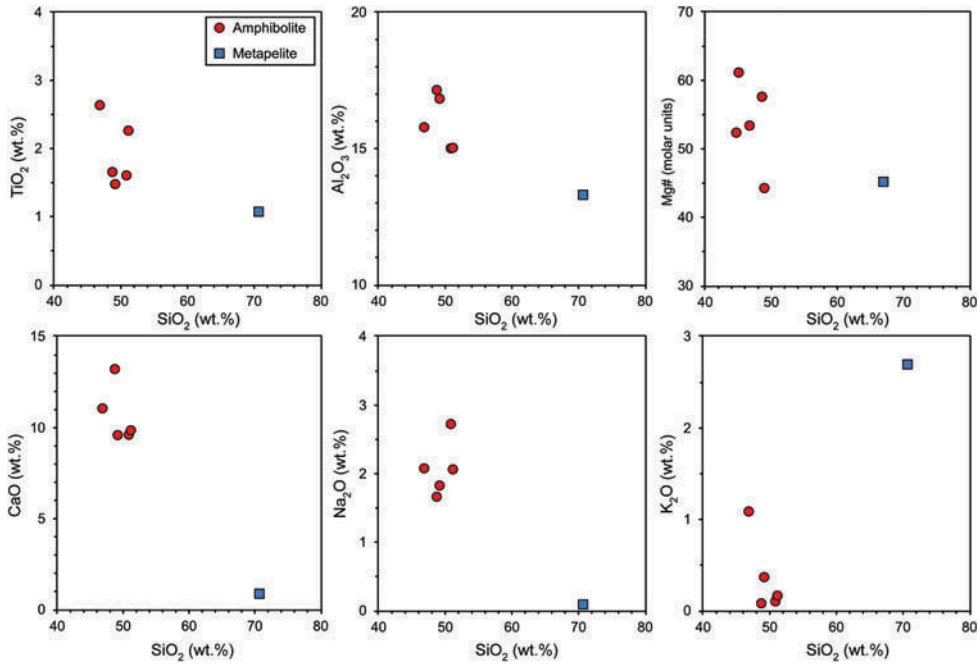

Figure 10. TiO_2, Al_2O_3, Mg#, CaO, Na_2O, and K_2O *versus* SiO_2 diagrams for amphibolites (circles) and metapelites (squares).

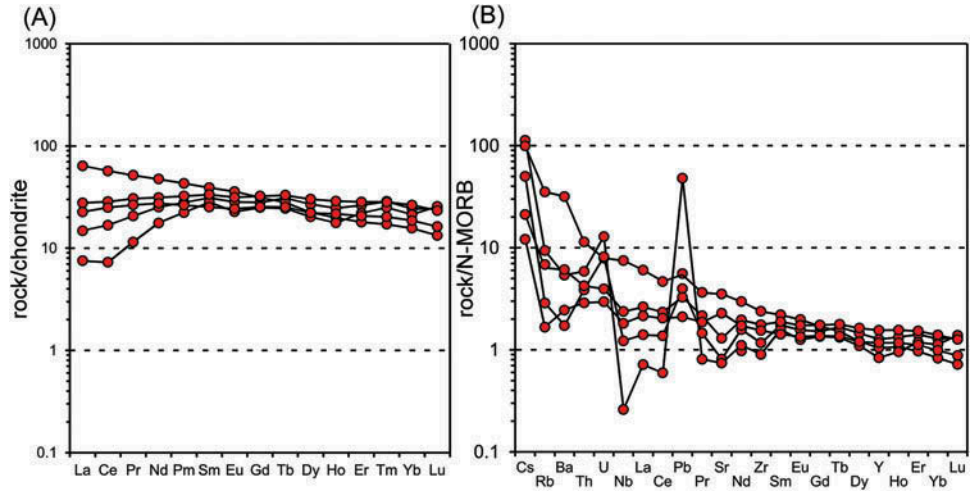

Figure 11. (A) REE and (B) element abundances of the studied amphibolites normalized to the chondrite (CI; McDonough and Sun 1995) and N-MORB (Sun and McDonough 1989), respectively.

Discussion

Origin of the protoliths

The composition and mineral associations of metapelitic rocks indicate a sedimentary protolith deposited at the Earth's surface. The intimate association of pelitic rocks and rocks of basaltic protolith is hence better explained as a volcano-sedimentary pile formed during contemporaneous volcanism and sedimentation in a basin. The tholeiitic basaltic (Figure 9) N-MORB affinity (Figure 11B) of the amphibolites suggests a deep-marine environment, likely a mid-ocean ridge, back-arc, or fore-arc basin. During effusion, the lava flows may have been contaminated by the sediments, explaining the anomalies in Pb and LILEs. However, chemical deviations from ideal N-MORB observed in the concentration of LILEs can be also explained by element mobility during pre-metamorphic (i.e. sea-floor) and metamorphic (i.e. deep-crust) fluid/rock interactions.

The MORB signature is also evident from tectonic discrimination diagrams for basaltic rocks using immobile

Table 5. Ar/Ar measurements.

Run	Watts	36Ar/^{39}Ar	%36Ar	^{40}Ar/^{39}Ar	Mol ^{39}Ar	% Step	%^{40}Ar*	Age (Ma)	±Age
CR-03, Run ID# 12676-01 (J = 0.0015471 ± 1.700000*10^{6})									
A	5.0	0.990510	0.3	145.41724	0.0400	1.6	33.1	366.09059	6.4
B	10	0.015829	12.8	59.16498	1.1916	49.2	93.5	158.01155	0.3
C	12.0	0.013801	14.8	59.03350	0.7684	31.7	94.4	157.67530	0.6
D	14.0	0.020932	10.2	58.91703	0.2253	9.3	91.3	157.37741	1.2
E	16.0	0.021800	9.9	58.59973	0.0829	3.4	90.9	156.56558	2.0
F	20.0	0.021338	9.9	58.33400	0.0911	3.8	91.1	155.88541	2.1
G	30.0	0.044563	4.7	51.70692	0.0227	0.9	80.4	138.83920	4.8
Integrate age								161.2	0.7
Plateau age							97.4	157.80000	0.6
CR-30, Run ID# 12678–01 (J = 0.0015476 ± 1.700000*10^{6})									
A	5.0	0.513152	0.4	54.94369	0.0602	5.9	26.6	147.23063	4.0
B	10.0	0.050733	12.4	54.56619	0.3878	37.8	80.4	146.25897	0.7
C	12.0	0.043423	15.1	54.56003	0.3475	33.9	83.1	146.24312	1.0
D	14.0	0.038989	17.9	54.70106	0.1176	11.5	85.0	146.60619	1.4
E	16.0	0.034481	24.0	56.26167	0.0711	6.9	87.7	150.61892	2.5
F	20.0	0.025184	28.1	58.89671	0.0330	3.2	91.5	157.37411	4.2
G	30.0	0.017771	44.6	64.10900	0.0085	0.8	95.6	170.66230	15.6
Integrate age								147.2	1.3
Plateau age							96.0	146.50000	1.1
CR-06, Run ID# 12677-01 (J = 0.0015474 ± 1.700000*10^{6})									
A	3.0	0.050920	0.0	55.00659	0.6700	1.9	78.5	147.37054	0.5
B	6.0	0.011986	0.0	58.89911	8.1972	23.1	94.3	157.35689	0.2
C	9.0	0.006635	0.0	58.86835	9.5328	26.9	96.8	157.27820	0.2
D	12.0	0.005466	0.0	58.93467	6.4287	18.1	97.3	157.44786	0.2
E	15.0	0.003407	0.0	58.98150	4.4691	12.6	98.3	157.56766	0.2
F	20.0	0.006657	0.0	59.08623	3.9823	11.2	96.8	157.83557	0.3
G	25.0	0.007652	0.0	59.00721	2.0066	5.7	96.3	157.63343	0.5
H	30.0	0.004559	0.1	59.28457	0.2000	0.6	97.8	158.34278	1.7
Integrate age								157.3	0.4
Plateau age							98.1	157.50000	0.4

elements (Figure 13). Within the V *versus* Cr diagram (Pearce 1982), the amphibolites clearly show a MORB affinity (Figure 13A). This affinity is also well defined in the Ti *versus* V diagram (Figure 13B; Shervais 1982). Small variations are observed (e.g. Figures 11B and 13B) possible due to assimilation of sediments and/or fluid–rock interactions.

Similar geochemical features in MORB-type amphibolites of the Cajamarca Complex and associated rocks of Ecuador have been reported by Restrepo-Pace (1992) and Cochrane *et al*. (2014). Cochrane *et al*. (2014) studied mafic rocks of Triassic magmatic age considered to be related to extensional tectonics in the continental margin or an intra/back-arc basin. While the tectonic setting of these and our studied rocks may be similar (i.e. an intra-arc or back-arc basin), the protolith ages are not necessarily comparable (see the 'Age of metamorphism' section).

Tectonic setting of metamorphism

The calculated peak-*T* pressure of approximately 8 kbar indicates depths down to approximately 26 km during prograde (burial + heating) metamorphism. The apparent geothermal gradient during peak-*T* conditions is 22°C/km, typical of intermediate *P*/*T* metamorphic field gradients (i.e. Barrovian type) generally considered collision related (e.g. Brown 2007, 2009). These data, together with the fact that the protolithic sediments and tholeiitic basaltic rocks of the metamorphic complex formed at an oceanic basin and followed a prograde *P*–*T* path involving burial and heating, are better conceptualized within a model of collision and tectonic shortening rather than tectonic extension. In addition, the strong syn-metamorphic ductile deformation (e.g. flattening and shear deformation with development of mylonitic foliation) of the metamorphic rocks (Figures 2 and 5) exclude (near-) static contact metamorphism of nearby igneous bodies, such as the Ibagué batholith that is only barely deformed.

Important to note, the Mesozoic–Tertiary tectonic evolution of the Central Cordillera was controlled by several strike-slip fault systems (e.g. Otú-Pericos, Romeral, etc.), the activity of which has amalgamated blocks of different ages and natures that were originally located far apart (e.g. Toussaint 1995; Bayona *et al*. 2010). In fact, intrusive contacts in the study area have not been observed, as a consequence of the intense activity of important strike-slip

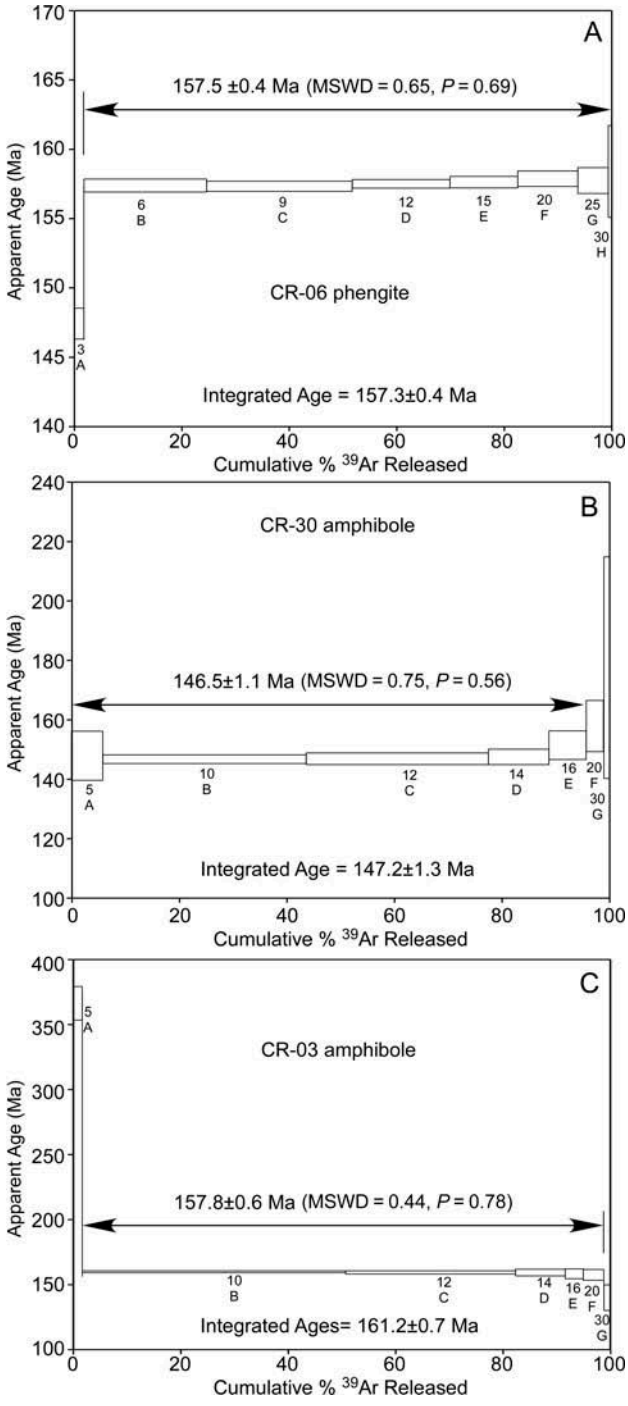

Figure 12. Ar/Ar age spectra for studied samples.

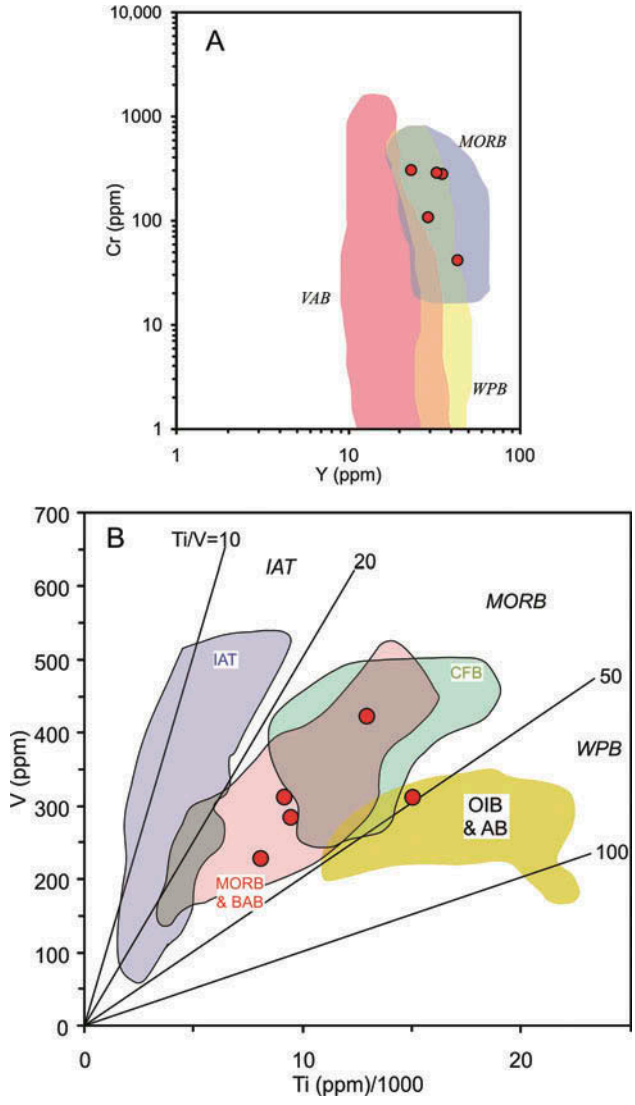

Figure 13. (A) Cr–Y diagram (Pearce 1982) for discrimination between MORB, volcanic-arc basalt (VAB), and within plate basalt (WPB); (B) Ti *versus* V diagram (Shervais 1982), showing the fields of island arc tholeiite (IAT), MORB, and back-arc basin basalt (BAB), continental flood basalt (CFB), and ocean-island (OIB) and alkali basalt (AB) fields after Rollinson (1993).

faults in the area (e.g. Mosquera *et al*. 1982; Gómez-Tapia and Bocanegra-Gómez, 1999).

In the scenario of tectonic shortening, collision, and strike-slip movement, oblique subduction and possible associated subduction erosion can be anticipated. Thus, an arc setting and an oblique subduction setting can yield the heat and the necessary shearing to produce the observed metamorphic rock package in a fore-arc position. However, the collision-related metamorphism would be expected by the combination of erosion and structural collapse of the fore-arc wedge into the trench, producing differences in the chemical compositions of the magma (e.g. Stern 2011 and references therein). These characteristics have not been described in the area and the position of these rocks was not in the trench (see the 'A potential Late Jurassic collision scenario' section). More data are needed to fully understand the tectonic setting of metamorphism. Besides, the textural/structural data of the studied rocks and the barely deformed nearby Ibague batholiths preclude considering contact metamorphism triggered by igneous intrusions as the cause of metamorphism.

Age of metamorphism

The ^{40}Ar-^{39}Ar results reported in this work record Late Jurassic ages (157.8 ± 0.6–146.5 ± 1.1 Ma).

Since stocks of the nearby Ibague batholith have Jurassic ages (K/Ar hornblende and biotite ages of 150–140 Ma; Vesga and Barrero 1978; Brook 1984, Ar/Ar hornblende and biotite ages of 183–147 Ma and U-Pb zircon ages of 166–169 Ma and 189 Ma; Villagómez *et al*. 2011), a Jurassic resetting of the well-established (Permian)Triassic orogenic metamorphic ages must be considered. However, the consistent $^{40}Ar/^{39}Ar$ plateaus implies that argon extracted from lower *T* domains and higher *T* domains in the dated crystals had the same isotopic composition. Partial Ar loss by heat from a nearby pluton would not have produced the plateaus. On the other hand, total Ar loss by a nearby pluton would explain the obtained plateaus, but they are inconsistent with the strong oriented fabric of the amphibolites. If heating by the pluton was so strong as to completely degas the amphibole, then the rock would have recrystallized under static amphibolite-facies conditions erasing the previous fabric.

The *P–T* calculated conditions at approximately 550–580ºC during metamorphism allow interpreting the Late Jurassic ages as cooling ages formed during decompression and cooling after the established peak metamorphic conditions. The peak temperature reached exceeds the blocking (closure) temperatures of muscovite-phengite (350–450°C; Purdy and Jäger 1976; Kirschner *et al*. 1996; Harrison *et al*. 2009) and amphibole (480–580°C, Harrison 1982; McDougall and Harrison 1999), but only in a few tens of Celcius above in the case of amphibole, suggesting that peak conditions were attained shortly before cooling at 158–147 Ma. Hence, we provide evidence for Jurassic Barrovian-type metamorphism in the Central Cordillera of Colombia for the first time. This age contrasts with the nominally (Permian)Triassic age of metamorphism in the Cajamarca Complex (Table 6). The new evidence of a Jurassic metamorphism presented in this contribution let us suggest that the common view of the metamorphic evolution of the Central Cordillera as a pre-Jurassic belt must be reviewed. The use of the term Cajamarca Complex to include the entire metamorphic rocks of the basement of the Central Cordillera seems inappropriate, and additional geochronological, geochemical, and metamorphic constraints are needed to understand the long-term evolution of this convergent continental margin.

Table 6. Summary of published ages of metamorphic rocks of the basement of the Central Cordillera (i.e. Cajamarca and other complexes).

Complex	Rock type	method	Ages (Ma)	Reference
Las Palmas migmatite	Migmatita	U-Pb	240 ± 10	Restrepo *et al*. (2009)
El Retiro	Amphibolite	Ar/Ar Amp	230 Ma	Vinasco *et al*. (2006)
El Retiro	Granulite	Sm/Nd isochron	226 ± 17	Ordoñez-Carmona (2001)
El Retiro	Granulite	K-Ar WR	251 ± 21	Restrepo *et al*. (1991)
Pescadero Gneiss	Gneiss	Rb/Sr WR Icochron	253 ± 10	Restrepo *et al*. (1991)
Ancón Schist	Schist	Rb/Sr WR Icochron	226 ± 4	Restrepo *et al*. (1991)
Cajamarca Complex	Chloritic schist	K-Ar-WR	61.0 ± 10	Núñez *et al*. (1979)
Cajamarca Complex	Qtz-sericite phyllite	K-Ar-WR	73.3 ± 2,5	Vesga and Barrero (1978)
Cajamarca Complex	Actinolite schist	K-Ar-WR	84.4 ± 10,0	Núñez *et al*. 1979
Cajamarca Complex	Gneiss	U-Pb Zrc	238–582	Villagómez *et al*. (2011)
Cajamarca Complex	Gneiss	Ar/Ar Hbl	155.6 ± 6.2	Villagómez *et al*. (2011)
Cajamarca Complex	Quarzite	U-Pb Zrc	231–1163	Villagómez *et al*. (2011)
Aberrojal Gneiss	Gneiss	Ar/Ar Bt	230 ± 0.2	Vinasco *et al*. (2006)
Manizales Gneiss	Gneiss	Ar/Ar Ms	228.7 ± 0.4	Vinasco *et al*. (2006)
Padua Amphibolite	Amphibolite	Ar/Ar Hbl	243 ± 4	Vinasco *et al*. (2006)
Padua Amphibolite	Amphibolite	Ar/Ar Hbl	246 ± 6	Vinasco *et al*. (2006)
Río Verde Gneiss	Gneiss	U-Pb Zrc	290–302	Vinasco *et al*. (2006)
Palmitas Gneiss	Gneiss	U-Pb Zrc	250	Vinasco *et al*. (2006)
Abejorral Gneiss	Gneiss	U-Pb Zrc	250–300	Vinasco *et al*. (2006)
Aberrojal Gneiss	Gneiss	Ar/Ar Bt	207 ± 5	González (1980)
Horizontes Gneiss	Gneiss	Ar/Ar Ms	211	Vinasco *et al*. (2006)
Nechí Gneiss	Gneiss	U-Pb SHRIMP	277.3 ± 3	Restrepo *et al*. (2011)
Santa Isabel Gneiss	Gneiss	U-Pb SHRIMP	226.7 ± 1.9	Restrepo *et al*. (2011)
Tierradentro	Amphibolite	K-Ar Hbl	171.0 ± 13	Vesga and Barrero (1978)
Tierradentro	Amphibolite	K-Ar Hbl	221.0 ± 10	Vesga and Barrero (1978)
Tierradentro	Amphibolite	K-Ar Hbl	226.0 ± 10	Vesga and Barrero (1978)
Tierradentro	Amphibolite	K-Ar WR	1360.0 ± 270	Vesga and Barrero (1978)

Note: WR = whole rock.

A potential Late Jurassic collision scenario

Based on palaeomagnetic data, Bayona *et al.* (2006, 2010) inferred that Jurassic terranes moved from south to north along the Andean margin until Early Cretaceous time. These terrane relocations are also supported by the distribution of Triassic marine sedimentary basins and development of palaeosols on continental Jurassic rocks (Bayona *et al.* 2006, 2010). The inferred transfers include those of the Ibague Batholith and other northern Colombian blocks, all of which are thought to have formed in northern Peru and Ecuador (Bayona *et al.* 2010). During the implied dextral slip of blocks, the Jurassic volcanic arc evolved from an extensional to a compressive system, as revealed by deformation of ca. 143 Ma granitoids of Ecuador (Aspden *et al.* 1992; Noble *et al.* 1997). It could be therefore suggested that metamorphism is linked to this tectonic scenario, where crustal thickening accompanying Late Jurassic orogeny may have occurred further south of the present position of the studied rock complex.

Between the Middle and Late Jurassic, the northwestern margin of South America, including Colombia and Ecuador, was affected by subduction of palaeo-Pacific plate(s) and multiple continental rifting events associated with the opening of the Caribbean (e.g. Figures 4 and 5 of Pindell and Kennan 2009; see also Kennan and Pindell 2009). Using these published reconstructions for the western margin of Pangea, our tectonic model for the evolution of the Cajamarca Complex is summarized in Figure 14. During this time interval, the basement of the Central Cordillera was located west of a rift system (Figure 14A and B), which eventually detached from the margin (Eastern Cordillera), possibly induced by slab rollback, forming a small oceanic basin where the protoliths of metapelite and metabasite accumulated. This oceanic basin had a fore-arc position, but separated the pre-Jurassic basement of the Central Cordillera from mainland Pangea. Jurassic magmatism took place along the eastern flank of the (future) Central Cordillera (Aspden *et al.* 1987), including the Ibagué batholith (Pindell and Kennan 2009; Villagómez *et al.* 2011). Late Jurassic transpression closed the oceanic basin triggered (local?) collision and dynamic–thermal metamorphism (Figure 14C). Serpentinites in the study area may represent fragments of this oceanic mantle lithosphere exhumed during the

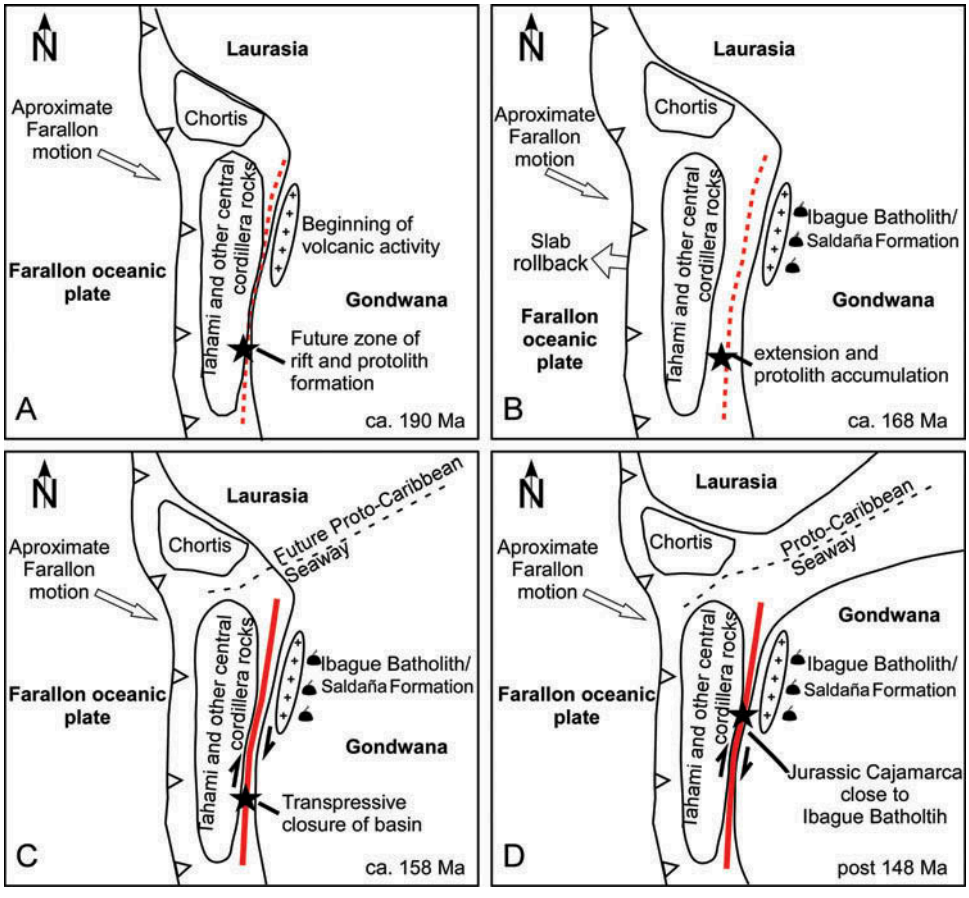

Figure 14. Proposed model for the tectonic evolution of the northwestern margin of Gondwana during the Jurassic (based on Pindell and Kennan 2009).

collision. A regional angular unconformity in the Late Jurassic on top of the volcanic Saldaña Formation (Toussaint 1995) may also be another consequence of collision. After all these processes and since the Jurassic to present, further northward displacements of the blocks approached the studied metamorphic package to the Ibagué Batholith (Figure 14D).

Conclusions

Our data open new perspectives for the evolution of the northwestern margin of Gondwana/South America. In the study area, nominally part of the (Permian)Triassic Cajamarca Complex of the Central Cordillera of Colombia, a package of strongly deformed amphibolites and intercalated layers of garnet-bearing pelitic schist is of Late Jurassic age (amphibole and one phengitic mica ^{40}Ar-^{39}Ar plateau ages of 147–158 Ma). The geochemistry of the amphibolites indicates basaltic protoliths of N-MORB affinities likely formed in a fore-arc setting. After a likely clockwise prograde (burial+heating) metamorphism, peak conditions attained 550–580°C and 8 kbar and evolved along a cooling and decompression path, indicating collision. Jurassic terrane collision including buoyant crustal element such as a volcanic arc or a formerly passive continental margin is inferred given that the studied supracrustal rock body was buried to mid-crustal levels of approximately 26 km depth. The present geological setting of the complex does not provide unambiguous clues for resolving which crustal elements were involved in the collision, for all the contacts with nearby geologic elements are tectonic (dextral strike-slip faults). Our Late Jurassic ages are not consistent with previously published Triassic ages of metamorphism in other parts of the Cajamarca Complex. However, (Permian)Triassic tectonic models for the Cajamarca Complex are characterized by extension, rifting, and mafic magma underplating, which is not consistent with compression and heating as indicated by the studied metapelites and amphibolites. Thus, it appears that the Cajamarca Complex, as presently defined, contains geologic elements of different age that record different tectonic events, including extension and compression. Hence, we propose that the studied amphibolites and metapelites have nothing to do with the Permian–Triassic Cajamarca Complex and instead represent a distinct collision–accretion event of Late Jurassic age which challenges the traditional tectonic views for the region.

Acknowledgements

The authors thank the constructive reviews of U. Martens and G. Bayona that substantially improved this article and editor R. Stern for editorial suggestions.

Funding

We appreciate the financial support from Spanish MICINN projects CGL2009-12446 and CGL2012-36263 and from the FAPA project from Vicerrectoria de Investigación (Uniandes).

References

Altenberger, U., and Concha, A.E., 2005, Late lower to early middle Jurassic arc magmatism in the northern Ibagué-Batholith/Colombia: Geología Colombiana, v. 30, p. 87–97.

Arancibia, G., Matthews, S., and Pérez de Arce, C., 2006, K–Ar and ^{40}Ar/^{39}Ar geochronology of supergene processes in the Atacama Desert, northern Chile: Tectonic and climatic relations: Journal of the Geological Society of London, v. 163, p. 107–118. doi:10.1144/0016-764904-161

Aspden, J.A., and Litherland, M., 1992, The geology and Mesozoic collisional history of the Cordillera Real, Ecuador: Tectonophysics, v. 205, p. 187–204. doi:10.1016/0040-1951(92)90426-7

Aspden, J.A., McCourt, W.J., and Brook, M., 1987, Geometrical control of subduction-related magmatism: The Mesozoic and Cenozoic plutonic history of Western Colombia: Journal of the Geological Society, v. 144, p. 893–905. doi:10.1144/gsjgs.144.6.0893

Barrero, D., and Vesga, C.J., 1976, Mapa geológico del cuadrángulo K 9, Armero y mitad sur del J 9, La Dorada. Escala 1:100.000: Bogotá, NJ, INGEOMINAS.

Bayona, G., Cardona, A., Jaramillo, C., Mora, A., Montes, C., Valencia, V., Ayala, C., Montenegro, O., and Ibañez, M., 2012, Early Paleogene magmatism in the northern Andes: Insights on the effects of Oceanic Plateau-Continent convergence: Earth and Planetary Science Letters, v. 331–332, p. 97–111. doi:10.1016/j.epsl.2012.03.015

Bayona, G., Garcia, D., and Mora, G., 1994, La Formación Saldaña: Un ejemplo de acumulación en una cuenca de retro-arco, *in* Etayo, F., ed., Estudios Geológicos del Valle Superior del Magdalena: Special Publication, Bogotá, Universidad Nacional y Ecopetrol, p. I1–I21.

Bayona, G., Jiménez, G., Silva, C., Cardona, A., Montes, C., Roncancio, J., and Cordani, U., 2010, Paleomagnetic data and K–Ar ages from Mesozoic units of the Santa Marta Massif: A preliminary interpretation for block rotations and translations: Journal of South American Earth Sciences, v. 29, no. 4, p. 817–831. doi:10.1016/j.jsames.2009.10.005

Bayona, G., Rapalini, A., and Costanzo-Alvarez, V., 2006, Paleomagnetism in Mesozoic rocks of the Northern Andes and its implications in Mesozoic Tectonics of Northwestern South America: Earth Planets and Space, v. 58, p. 1255–1272. doi:10.1186/BF03352621

Brook, M., 1984, New radiometric age data from SW Colombia. Ingeominas-Mision Britanica: Colombia, British Geological Service. Report, 10.

Brown, M., 2007, Metamorphic conditions in orogenic belts: A record of secular change: International Geology Review, v. 49, p. 193–234. doi:10.2747/0020-6814.49.3.193

Brown, M., 2009, Metamorphic patterns in orogenic systems and the geological record: London, Geological Society, Special Publication, v. 318, p. 37–74.

Bustamante, A., Juliani, C., Hall, C.M., and Essene, E.J., 2011, ^{40}Ar-^{39}Ar ages from blueschists of the Jambaló region, Central Cordillera of Colombia: Implications on the styles of accretion in the Northern Andes: Geologica Acta, v. 9, p. 351–362.

Bustamante, C., Agustín Cardona, A., Bustamante, A., and Valencia, V., 2014, U-Pb zircon ages from bi-modal magmatic rocks in the southeastern central Cordillera of the Colombian Andes: Implications for regional correlations and tectonic models during Pangea assembly, *in* 9th South American Symposium on Isotope Geology - 9th SSAGI, 6–9April: São Paulo.

Cardona, A., Valencia, V., Garzón, A., Montes, C., Ojeda, G., Ruiz, J., and Weber, M., 2010, Permian to Triassic I to S-type magmatic switch in the northeast Sierra Nevada de Santa Marta and adjacent regions, Colombian Caribbean: Tectonic setting and implications within Pangea paleogeography: Journal of South American Earth Sciences, v. 29, p. 772–783. doi:10.1016/j.jsames.2009.12.005

Cediel, F., Shaw, R.P., and Caceres, C., 2003, Tectonic assembly of the Northern Andean Block, *in* Bartolini, C., Buffler, R.T., and Blickwede, J., eds., The Circum-Gulf of Mexico and the Caribbean: Hydrocarbon habitats, basin formation, and plate tectonics: American Association of Petroleum Geologists Memoir, v. 79, p. 815–848.

Cochrane, R., Spikings, R.A., Gerdes, A., Ulianov, A., Mora, A., Villagómez, D., Putlitz, B., and Chiaradia, M., 2014, Permo-Triassic anatexis, continental rifting and the disassembly of western Pangaea: Lithos, v. 190–191, p. 383–402. doi:10.1016/j.lithos.2013.12.020

Coggon, R., and Holland, T.J.B., 2002, Mixing properties of phengitic micas and revised garnet-phengite thermobarometers: Journal of Metamorphic Geology, v. 20, p. 683–696. doi:10.1046/j.1525-1314.2002.00395.x

Connolly, J.A.D., 2005, Computation of phase equilibria by linear programming: A tool for geodynamic modeling and its application to subduction zone decarbonation: Earth and Planetary Science Letters, v. 236, p. 524–541. doi:10.1016/j.epsl.2005.04.033

Dale, J., Powell, R., White, R.W., Elmer, F.L., and Holland, T.J.B., 2005, A thermodynamic model for Ca-Na clinoamphiboles in Na_2O-CaO-FeO-MgO-Al_2O_3-SiO_2-H_2O-O for petrological calculations: Journal of Metamorphic Geology, v. 23, p. 771–791. doi:10.1111/j.1525-1314.2005.00609.x

Fleck, R.J., Sutter, J.F., and Elliot, D.H., 1977, Interpretation of discordant $^{40}Ar/^{39}Ar$ age-spectra of mesozoic tholeiites from Antarctica: Geochimica et Cosmochimica Acta, v. 41, p. 15–32. doi:10.1016/0016-7037(77)90184-3

Gomez-Tapia, J., and Bocanegra-Gomez, A., 1999, Estudio geológico-estructural de la Falla Otú-Pericos al W de la Ciudad de Ibagué. Unpublished Report: Manizales, Universidad de Manizales.

González, H., 1980, Geología de las Planchas 167 (Sonson) e 187 (Salamina): Boletín Geológico de Ingeominas, Informe 1760.

González, H., 2001, Mapa Geológico del departamento de Antioquia. Escala 1:400.000. Memoria explicativa: Medellín, AN, Ingeominas.

González, H., Nuñez, A., and Paris, G., 1988, Mapa Geológico de Colombia. Memoria explicativa: Bogotá, Ingeominas.

Govindaraju, K., 1994, 1994 Compilation of working values and sample description for 383 geostandards: Geostandards and Geoanalytical Research, v. 18, p. 1–158. doi:10.1111/j.1751-908X.1994.tb00502.x

Harrison, T.M., 1982, Diffusion of 40Ar in hornblende: Contributions to Mineralogy and Petrology, v. 78, p. 324–331. doi:10.1007/BF00398927

Harrison, T.M., Célérier, J., Aikman, A.B., Hermann, J., and Heizler, M.T., 2009, Diffusion of ^{40}Ar in muscovite: Geochimica et Cosmochimica Acta, v. 73, p. 1039–1051. doi:10.1016/j.gca.2008.09.038

Hey, M.H., 1954, A new review of the chlorites: Mineralogical Magazine, v. 30, p. 277–292. doi:10.1180/minmag.1954.030.224.01

Holland, T.J.B., Baker, J.M., and Powell, R., 1998, Mixing properties and activity-composition relationships of chlorites in the system MgO–FeO–Al_2O_3–SiO_2–H_2O: European Journal of Mineralogy, v. 10, p. 395–406. doi:10.1127/ejm/10/3/0395

Holland, T.J.B., and Powell, R., 1998, An internally consistent thermodynamic data set for phases of petrological interest: Journal of Metamorphic Geology, v. 16, p. 309–343. doi:10.1111/j.1525-1314.1998.00140.x

Horton, B.K., Saylor, J.E., Nie, J., Mora, A., Parra, M., Reyes-Harker, A., and Stockli, D.F., 2010, Linking sedimentation in the northern Andes to basement configuration, Mesozoic extension, and Cenozoic shortening: Evidence from detrital zircon U-Pb ages, Eastern Cordillera, Colombia: Geological Society of America Bulletin, v. 122, no. 9–10, p. 1423–1442.

Kennan, L., and Pindell, J.L., 2009, Dextral shear, terrane accretion and basin formation in the Northern Andes: Best explained by interaction with a Pacific-derived Caribbean Plate?, *in* James, K.H., Lorente, M.A., and Pindell, J.L., eds., The origin and evolution of the Caribbean plate: Geological Society, London, Special Publications, v. 328, p. 487–531.

Kerr, A.C., Marriner, G.F., Tarney, J., Nivia, A., Saunders, A.D., Thirlwall, M.F., and Sinton, C.W., 1997, Cretaceous basaltic terranes in western Colombia: Elemental, chronological and Sr–Nd isotopic constraints on petrogenesis: Journal of Petrology, v. 38, p. 677–702. doi:10.1093/petroj/38.6.677

Kerr, A.C., and Tarney, J., 2005, Tectonic evolution of the Caribbean and northwestern South America: The case for accretion of two Late Cretaceous oceanic plateaus: Geology, v. 33, p. 269–272. doi:10.1130/G21109.1

Kirschner, D.L., Cosca, M.A., Masson, H., and Hunziker, J.C., 1996, Staircase $^{40}Ar/^{39}Ar$ spectra of fine-grained white mica: Timing and duration of deformation and empirical constraints on argon diffusion: Geology, v. 24, p. 747–750. doi:10.1130/0091-7613(1996)024<0747:SAASOF>2.3.CO;2

Le Maitre, R.W., Bateman, P., Dudek, A., Keller, J., Lameyre, J., Le Bas, M.J., Sabine, P.A., Schmid, R., Sorensen, H., Streckeisen, A., Woolley, A.R., and Zanettin, B., 1989, A classification of igneous rocks and glossary of terms: Oxford, Blackwell.

Leake, B.E., Woolley, A.R., Arps, C.E.S., Birch, W.D., Gilbert, M. C., Grice, J.D., Hawthorne, F.C., Kato, A., Kisch, H.J., Krivovichev, V.G., Linthout, K., Laird, J., Mandarino, J.A., Maresch, W.V., Nickel, E.H., Rock, N.M.S., Schumacher, J. C., Smith, D.C., Stephenson, N.C.N., Ungaretti, L., Whittaker, E.J.W., and Touzhi, G., 1997, Nomenclature of amphiboles: Report of the subcommittee on amphiboles of the International Mineralogical Association, Commission on new minerals and mineral names: American Mineralogist, v. 82, p. 1019–1037.

Maya, M., and González, H., 1995, Unidades litodémicas en la Cordillera Central de Colombia: Boletín Geológico, Ingeominas, v. 35, no. 2–3, p. 43–57.

McDonough, W.F., and Sun, S.S., 1995, The composition of the earth: Chemical Geology, v. 120, no. 3–4, p. 223–253. doi:10.1016/0009-2541(94)00140-4

McDougall, I., and Harrison, T.M., 1999, Geochronology and thermochronology by the $^{40}Ar/^{39}Ar$ method: Oxford, Oxford University Press, 288 p.

Mosquera, D., Núñez, A., and Vesga, C.J., 1982, Mapa geológico preliminar de la Plancha 244-Ibagué. Escala 1:100000: Bogotá, INGEOMINAS.

Nelson, W.H., 1962, Contribución al conocimiento de la Cordillera Central de Colombia sección entre Ibagué y Armenia: Boletín Geológico, Servicio Geológico Nacional, v. 10, no. 13, p. 161–202.

Newton, R.C., Charlu, T.V., and Kleppa, O.J., 1980, Thermochemistry of the high structural state plagioclases: Geochimica et Cosmochimica Acta, v. 44, p. 933–941. doi:10.1016/0016-7037(80)90283-5

Nivia, A., Marriner, G.F., Kerr, A.C., and Tarney, J., 2006, The Quebradagrande complex: A Lower Cretaceous ensialic marginal basin in the Central Cordillera of the Colombian Andes: Journal of South American Earth Sciences, v. 21, p. 423–436. doi:10.1016/j.jsames.2006.07.002

Noble, S.R., Aspden, J.A., and Jemielita, R., 1997, Northern Andean crustal evolution: New U-Pb Geochronological constraints from Ecuador: Geological Society of America Bulletin, v. 109, p. 789–798. doi:10.1130/0016-7606(1997)109<0789:NACENU>2.3.CO;2

Núñez, A., González, H., and Linares, E., 1979, Nuevas edades radiométricas de los esquistosverdes del Grupo Cajamarca: Medellín, AN, Publicación Especial de Geología, Universidad Nacional, v. 23, p. 1–18.

Núñez Tello, A., 2001, Mapa geológico del departamento del Tolima: Geología, recursos geológicos y amenazas geológicas, 1:250.000, memoria explicativa: Bogotá, INGEOMINAS.

Ordoñez-Carmona, O., 2001, Caracterização isotópica Rb-Sr e Sm-Nd dos principais eventos magmáticos nos Andes Colombianos [Ph.D. thesis]: Brasília, Universidade de Brasilia, 176 p.

Pearce, J.A., 1982, Trace element characteristics of lavas from destructive plate boundaries, *in* Thorpe, R.S., ed., Andesites: Chichester, Wiley, p. 525–548.

Peccerillo, A., and Taylor, S.R., 1976, Geochemistry of Eocene calc-alkaline volcanic-rocks from Kastamonu area, Northern Turkey: Contributions to Mineralogy and Petrology, v. 58, no. 1, p. 63–81.

Pindell, J., and Kennan, L., 2009, Tectonic evolution of the Gulf of Mexico, Caribbean and northern South America in the mantle reference frame: An update, *in* James, K.H., Lorente, M.A., and Pindell, J.L., eds., The origin and evolution of the Caribbean Plate: Geological Society of London, Special Publications, v. 328, p. 1–55.

Purdy, J.W., and Jäger, E., 1976, K–Ar ages on rock-forming minerals from the Central Alps: Mere Ist Geol Mineral University of Padova, v. 30, p. 1–32.

Renne, P.R., Deino, A.L., Walter, R.C., Turrin, B.D., Swisher, C. C., Becker, T.A., Curtis, G.H., Sharp, W.D., and Jaouni, A., 1994, Intercalibration of astronomical and radioisotopic time: Geology, v. 22, p. 783–786. doi:10.1130/0091-7613(1994)022<0783:IOAART>2.3.CO;2

Restrepo, J., and Toussaint, J., 1982, Metamorfismos superpuestos en la Cordillera Central de Colombia, *in* V Congreso Latino-Americano de Geologia, Buenos Aires, Asociación Geológica Argentina, p. 505–512.

Restrepo, J.J., Ordoñez-Carmona, O., Armstrong, R., and Pimentel, M.M., 2011, Triassic metamorphism in the northern part of the Tahamí Terrane of the central cordillera of Colombia: Journal of South American Earth Sciences, v. 32, p. 497–507. doi:10.1016/j.jsames.2011.04.009

Restrepo, J.J., Ordoñez-Carmona, O., Martens, U., and Correa, A.M., 2009, Terrenos, Complejos y Provincias en la Cordillera Central Colombiana: Boletin de Ciencias de la Tierra, v. 9, no. 2, p. 49–56.

Restrepo, J.J., and Toussaint, J.F., 1988, Terranes and continental accretion in the Colombian Andes: Episodes, v. 7, p. 189–193.

Restrepo, J.J., Toussaint, J.F., González, H., Cordani, U., Kawashita, K., Linares, E., and Parica, C., 1991, Precisiones geocronológicas sobre el occidente colombiano, *En* Simposio sobre magmatismo andino y su marco tectónico: Manizales, Memorias, Universidad de Caldas, Tomo I, p. 1–22.

Restrepo-Pace, P.A., 1992, Petrotectonic characterization of the Central Andean Terrane, Colombia: Journal of South American Earth Sciences, v. 5, p. 97–116. doi:10.1016/0895-9811(92)90062-4

Rieder, M., Cavazzini, G., D'Yakonov, Y.S., Frank-Kamenetskii, V.A., Gottardi, G., Guggenheim, S., Koval, P.V., Muller, G., Neiva, A.M.R., Radoslovich, E.W., Robert, J.-L., Sassi, F.P., Takeda, H., Weiss, Z., and Wones, D.R., 1998, Nomenclature of the Micas: IMA Mica subcommittee report: Canadian Mineralogist, v. 36, p. 905–912.

Rollinson, H.R., 1993, Using geochemical data: Evaluation, presentation, interpretation: Longman Scientific and Technical, 352 p.

Sarmiento-Rojas, L.F., Van Wess, J.D., and Cloetingh, S., 2006, Mesozoic transtensional basin history of the Eastern Cordillera, Colombian Andes: Inferences from tectonic models: Journal of South American Earth Sciences, v. 21, p. 383–411. doi:10.1016/j.jsames.2006.07.003

Sepulveda, R., and Saldarriaga, S., 1980, Metamorfismo de las rocas del oriente del municipio de Caldas (Antioquia). Monograph: Medellín, AN, Universidad Nacional de Colombia.

Shervais, J.W., 1982, Ti-V plots and the petrogenesis of modern and ophiolitic lavas: Earth and Planetary Science Letters, v. 59, p. 101–118. doi:10.1016/0012-821X(82)90120-0

Stern, C.R., 2011, Subduction erosion: Rates, mechanisms, and its role in arc magmatism and the evolution of the continental crust and mantle: Gondwana Research, v. 20, p. 284–308. doi:10.1016/j.gr.2011.03.006

Sun, S.S., and McDonough, W.F., 1989, Chemical and isotopic systematics of oceanic basalts; implications for mantle composition and processes, *in* Saunders, A.D., and Norry, M.J., eds., Magmatism in the ocean basins geological society special publications: London, Geological Society of London, p. 313–345.

Toussaint, J.F., 1993, Evolución Geológica de Colombia. Precámbrico-Paleozoico: Medellín, AN, Universidad Nacional de Colombia, 229 p.

Toussaint, J.F., 1995, Evolución Geológica de Colombia durante el Triásico y el Jurásico: Medellín, AN, Universidad Nacional de Colombia, 23 p.

Toussaint, J.F., and Restrepo, J.J., 1989, Acreciones sucesivas en Colombia: Un nuevo modelo de evolución geológica, *in* Memorias V. Congreso Colombiano de Geología: Bucaramanga, Ingeominas, v. 1, p. 127–146.

Vesga, C., and Barrero, D., 1978, Edades K/Ar en rocas ígneas y metamórficas de la Cordillera Central de Colombia y su implicación geológica, *in* II Congreso Colombiano de Geología, Bogotá, Universidad Nacional, Abstract, p. 21–31.

Villagómez, D., Spikings, R., Magna, T., Kammer, A., Winkler, W., and Beltrán, A., 2011, Geochronology, geochemistry and tectonic evolution of the Western and Central cordilleras of

Colombia: Lithos, v. 125, p. 875–896. doi:10.1016/j.lithos.2011.05.003

Vinasco, C.J., Cordani, U.G., González, H., Weber, M., and Pelaez, C., 2006, Geochronological, isotopic, and geochemical data from Permo-Triassic granitic gneisses and granitoids of the Colombian Central Andes: Journal of South American Earth Sciences, v. 21, p. 355–371. doi:10.1016/j.jsames.2006.07.007

Whitney, D.L., and Evans, B.W., 2010, Abbreviations for names of rock-forming minerals: American Mineralogist, v. 95, p. 185–187.

Winchester, J.A., and Floyd, P.A., 1977, Geochemical discrimination of different magma series and their differentiation products using immobile elements: Chemical Geology, v. 20, p. 325–343. doi:10.1016/0009-2541(77)90057-2